Sema3d controls collective endothelial cell migration by distinct mechanisms via Nrp1 and PlxnD1

Mailin Julia Hamm,[1,2] Bettina Carmen Kirchmaier,[3,4] and Wiebke Herzog[1,2]

[1]Cells-in-Motion Cluster of Excellence, University of Muenster, 48149 Muenster, Germany
[2]Max Planck Institute for Molecular Biomedicine, 48149 Muenster, Germany
[3]Institute of Cell Biology and Neuroscience and [4]Buchmann Institute for Molecular Life Sciences, University of Frankfurt, 60438 Frankfurt, Germany

During cardiovascular development, tight spatiotemporal regulation of molecular cues is essential for controlling endothelial cell (EC) migration. Secreted class III Semaphorins play an important role in guidance of neuronal cell migration and were lately linked to regulating cardiovascular development. Recently, *SEMA3D* gene disruptions were associated with cardiovascular defects in patients; however, the mechanisms of action were not revealed. Here we show for the first time that Sema3d regulates collective EC migration in zebrafish through two separate mechanisms. Mesenchymal Sema3d guides outgrowth of the common cardinal vein via repulsion and signals through PlexinD1. Additionally, within the same ECs, we identified a novel function of autocrine Sema3d signaling in regulating Actin network organization and EC morphology. We show that this new function requires Sema3d signaling through Neuropilin1, which then regulates Actin network organization through RhoA upstream of Rock, stabilizing the EC sheet. Our findings are highly relevant for understanding EC migration and the mechanisms of collective migration in other contexts.

Introduction

Cardiovascular development requires coordinated specification and migration of endothelial cells (ECs) and depends on the tight spatiotemporal regulation of attractive and repulsive guidance cues. Misregulation of these cues can result in improper EC guidance and developmental defects and has implications for disease etiologies in the adult organism.

The Class III Semaphorins are a group of seven secreted proteins: Sema3a, b, c, d, e, f, and g. They have been shown to act as guidance cues and can have repulsive or attractive functions (Raper, 2000). Class III Semaphorins were first discovered as axon guidance molecules (Kolodkin et al., 1992; Luo et al., 1993) and later were shown to play an important role in cardiovascular morphogenesis (Gu and Giraudo, 2013). Loss of SEMA3C in mice results in aortic arch and outflow tract septation defects (Feiner et al., 2001), whereas SEMA3E is required for intersomitic artery patterning (Gu et al., 2005; Meadows et al., 2012). Recently, SEMA3D has been shown to be necessary for pulmonary vein development and pulmonary venous connections in mice (Degenhardt et al., 2013). In addition, disruptions in the *SEMA3D* gene in human patients resulted in congenital heart defects and anomalous pulmonary vein formations (Degenhardt et al., 2013; Sanchez-Castro et al., 2015). These analyses of SEMA3D deficiencies in mice and humans, however, were confined to phenotypic descriptions and failed to elucidate the mechanisms by which SEMA3D fulfills its diverse functions. Sema3d has been shown to inhibit (Aghajanian et al., 2014) or promote (Foley et al., 2015) cell migration. These contrary functions could be caused by distinct spatiotemporal gene expression regulation, but also by signaling through different receptors. Class III Semaphorins can signal through receptors of the Neuropilin (Nrp) and Plexin (Plxn) families in various combinations (Gu and Giraudo, 2013). However, it is unknown how differentially regulated Sema3d acts in vivo to elicit distinct endothelial responses.

The technical difficulties of addressing this question stem from the inaccessibility of early embryonic development and the limitations of time- and tissue-specific knockout strategies. Therefore, we used the translucent and externally developing model organism zebrafish for the analysis of vascular development by endothelial-specific transgenic fluorophore expression (Schuermann et al., 2014). The zebrafish vasculature has high structural homology with other vertebrates (Isogai et al., 2001), and most signaling pathways are highly conserved (Ellertsdóttir et al., 2010). We use the developing common cardinal vein (CCV) as a model for collective EC migration during cardiovascular morphogenesis (Helker et al., 2013). The bilateral CCVs, which connect the venous system to the heart, develop as open-ended tubes from the cardinal veins and extend ventrally as sin-

Correspondence to Wiebke Herzog: wiebke.herzog@uni-muenster.de

Abbreviations used: AS, antisense; CCV, common cardinal vein; CRISPR, clustered regularly interspaced short palindromic repeats; Ctr, control; EC, endothelial cell; gRNA, guide RNA; hpf, hours post fertilization; HUVEC, human umbilical vein endothelial cell; LLP, lateral line primordium; MO, morpholino; SE, sense; Se, intersegmental vessel; VegfR, Vegf receptor; WT, wild type; ZO-1, zonula occludens 1.

The Rockefeller University Press $30.00
J. Cell Biol. Vol. 215 No. 3 415–430
https://doi.org/10.1083/jcb.201603100

gle EC sheets (Fig. 1, A and B). Finally, the CCVs connect to the endocardium and enclose their entire lumen at 50 h post fertilization (hpf). CCV ECs migrate actively as a collective cell sheet, serving further as a model for collective cell migration (Fig. 1 C and Videos 1 and 3).

To elucidate the mechanisms by which Sema3d fulfills its diverse functions in cardiovascular morphogenesis, we generated Sema3d-deficient zebrafish embryos. We performed morpholino (MO)-mediated gene knockdown and also generated zebrafish *sema3d* mutants using clustered regularly interspaced short palindromic repeats (CRISPR)/Cas9-mediated genome editing. We observed two phenotypes upon *sema3d* knockdown: first, a significantly shorter but wider CCV; and second, impaired collective and directional migration resulting in a disrupted EC sheet with impaired cell morphology. By using time- and tissue-specific knockdown as well as Sema3d receptor analysis, we showed that Sema3d elicits its differential functions by signaling through different receptors. Whereas mesenchymal Sema3d controls CCV outgrowth by signaling through PlxnD1 via repulsion, EC-specific Sema3d regulates Actin network organization and junction formation in the leading edge of collectively migrating ECs. There, Sema3d signals through Nrp1 via RhoA and Rock in an autocrine manner, facilitating consistent cell sheet organization.

Results

Sema3d is required for vascular development

To assess the role of Sema3d in cardiovascular morphogenesis of zebrafish embryos, we used MO-mediated blocking of translation (Sato et al., 2006) as well as CRISPR/Cas9-mediated genome editing (Hwang et al., 2013; Jao et al., 2013; Fig. S1, A–C). We identified three different mutations in the *sema3d* gene (10-, 14-, and 26-bp deletions) from CRISPR/Cas9 targeting, which all resulted in a premature stop codon and a predicted truncated protein product. Homozygous mutant offspring of all three different alleles showed the same phenotype. Therefore we focused on the 14-bp deletion allele *sema3d*^{mu268} (Fig. S1 B). Morphologically, *sema3d* morphants and mutants exhibit a thinned-yolk extension and occasionally a bent tail (Fig. S2 A).

To analyze vascular development, we performed confocal imaging of embryos with vascular-specific GFP expression (*Tg(kdrl:EGFP)*^{s843}). EC migration was impaired during CCV as well as intersegmental vessel (Se) development in *sema3d* morphants and mutants (Fig. 1, D–H; Fig. S2, E and F; and Fig. S3 A). Ses were stalled at the horizontal myoseptum and failed to migrate up to the dorsal longitudinal anastomotic vessel (DLAV). In rare cases, ECs did migrate up to the DLAV but lost connections to the Ses.

MO knockdown of *sema3d* was previously reported to cause impaired migration of the cardiac neural crest (Sato et al., 2006). Accordingly, we observed a mild reduction of flow at 30 hpf, but no changes of heartbeat, and a reduction in heart size, which became compensated by 50 hpf in *sema3d* morphants and mutants (Fig. S1 D).

Sema3d regulates collective EC migration by controlling CCV width and EC sheet organization

To investigate Sema3d function in collective EC migration, we analyzed CCV development in *Tg(kdrl:EGFP)*^{s843} embryos. We showed that both *sema3d* morphants and mutants failed to form a proper CCV (Fig. 1, D–H; and Fig. S2 E). CCV length was significantly reduced by ∼40% in morphants and mutants, whereas the CCV front width was nearly doubled at 30 hpf (Fig. 1, E, G, and H). We measured the CCV outgrowth angle and showed that Sema3d-deficient embryos exhibited a fanned-out CCV outgrowth. Whereas in control (Ctr) MO and wild-type (WT) embryos, the CCV ECs migrated out at a nearly orthogonal angle from the anterior and posterior cardinal vein, this angle was shifted by ∼20° upon knockdown, resulting in a widened CCV (Fig. S2 D).

In addition to this phenotype of increased CCV width, we identified a second phenotype exhibiting lesions in the leading edge of the EC sheet. For a more detailed investigation of cell morphology and especially Actin polymerization in the leading edge, we generated the transgenic line *Tg(fli1a:lifeactEGFP)*^{mu240}. We used the *fli* promoter to drive the Lifeact marker (Riedl et al., 2008) for visualization of F-Actin in endothelial and blood cells. Ctr morphants showed an ordered cell sheet with intact cell–cell contacts, whereas *sema3d* morphants and mutants showed a disorganized cell sheet with lesions (Fig. 1 F).

This disorganized cell sheet could be caused by a reduced number of cells. Thus, we investigated the CCV cell number, which was not affected before 32 hpf in *sema3d* morphants and mutants (Fig. S2 B). Because the two described phenotypes already occurred before 30 hpf, the reduced cell number cannot be causative, but EC migration itself might be impaired. Because Sema3d deficiency affected not only the CCV but also Se outgrowth, we investigated whether the stalled Se phenotype might be caused by reduced cell number or reduced sprouting. We quantified EC numbers at 30 hpf and sprouting events at 22 hpf (Fig. S3, B and C). Neither sprouting nor cell number was impaired in *sema3d* morphants or mutants, indicating that the stalled Se phenotype is also caused by impaired EC migration.

Based on these findings, we further investigated the migrational parameters of single CCV ECs from 28 to 32 hpf (Fig. 1, I and J; and Video 1 and 2). We found that neither the track length nor the migration speed was altered by Sema3d deficiency (Fig. 1, I and J). However, we observed changes in the outgrowth orientation, which we measured by determining the angle of the migration tracks relative to the perpendicular. We showed that this angle was on average more than doubled upon loss of Sema3d, which led to the fanned-out phenotype (Fig. 1 J). Moreover, in Ctr morphants, the ECs migrated ventrally in a highly directional manner. In contrast, upon *sema3d* knockdown, ECs changed direction and made detours. To quantify the altered directionality, we measured the migration track displacement length. In Ctr morphants, the EC track displacement amounted to 64 µm over 4 h, whereas in Sema3d-deficient embryos it was reduced to 48 µm (Fig. 1 J).

In sum, we observed two phenotypes upon loss of Sema3d: first, fanned-out cell migration tracks, leading to a shorter but wider CCV; and second, impaired collective and directional migration combined with a disrupted EC sheet (Fig. 1 K).

Sema3d is localized in the mesenchyme next to the CCV and in the ECs of the CCV leading edge

To understand these two distinct phenotypes of CCV collective migration upon *sema3d* knockdown, we investigated Sema3d

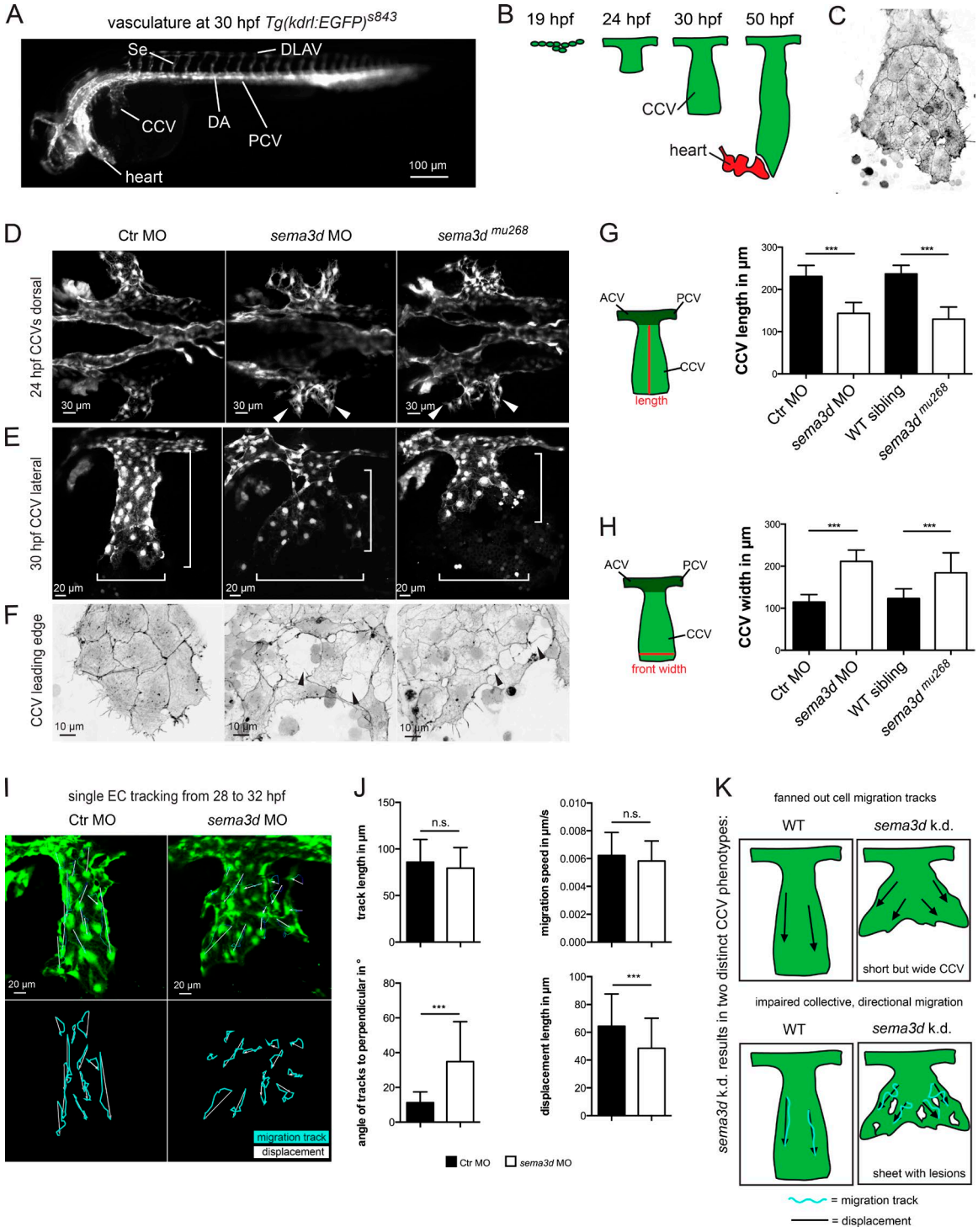

Figure 1. **Sema3d regulates collective EC migration by controlling CCV width and EC sheet organization.** (A) Vasculature of a 30-hpf-old zebrafish embryo visualized by GFP expression of *Tg(kdrl:EGFP)*^{s843}. (B) Illustration of CCV development. (C) CCV ECs migrate as a collective cell sheet; F-Actin visualized by GFP expression of *Tg(fli1a:lifeactEGFP)*^{mu240} at 32 hpf. (D–F) CCV development is impaired in *sema3d* morphants and mutants. (D) Widened CCV outgrowth upon Sema3d loss at 24 hpf (white arrowheads); confocal projections of *Tg(kdrl:EGFP)*^{s843} embryos. (E) Shorter but wider CCVs of *sema3d* morphants and mutants at 30 hpf (white brackets). (F) The CCV cell sheet exhibits lesions (black arrowheads) in the leading edges of 30-hpf Sema3d-deficient *Tg(fli1a :lifeactEGFP)*^{mu240} embryos. Confocal projections were color-inverted. (G) Quantification of CCV length shows a shortening in *sema3d* morphants and mutants at 30 hpf (each $n = 25$). (H) Quantification of CCV front width shows an increase in *sema3d* morphants and mutants at 30 hpf (each $n = 18$). (I and J) Tracking of single CCV EC migration from 28 to 32 hpf. (I) Confocal projections at 32 hpf with migration tracks (turquoise lines) and displacement distance (white arrows). (J) Quantification of migration parameters (each condition 84 cells and 14 cells per embryo/movie). Track length and migration speed are not impaired in *sema3d* morphants. In contrast, track displacement length is reduced and the angles of tracks to the perpendicular are increased in *sema3d* morphants compared with Ctr morphants, leading to a fanned-out CCV. (K) Model of *sema3d* knockdown (k.d.) representing the two distinct phenotypes: first, fanned-out cell migration tracks leading to a shorter but wider CCV; second, impaired collective and directional migration and a disrupted EC sheet. DA, dorsal aorta; ACV, anterior cardinal vein; PCV, posterior cardinal vein. ***, $P < 0.001$; n.s., not significant. Error bars indicate SD.

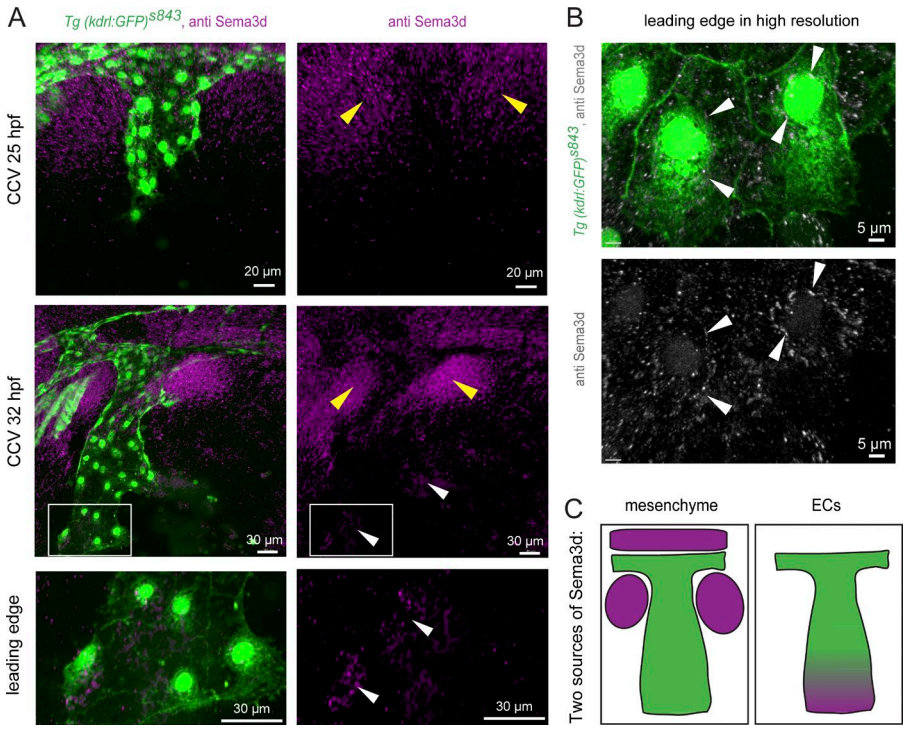

Figure 2. **Sema3d is localized in the mesenchyme next to the CCV and in the ECs of the CCV leading edge.** (A) Lateral confocal projections of *Tg(kdrl:EGFP)*^{s843} embryos at 25 and 32 hpf stained for Sema3d protein expression. Sema3d is localized in the mesenchyme next to the CCV (yellow arrowheads). At 32 hpf, Sema3d is additionally expressed in the CCV leading edge (white arrowheads). Magnification of the leading edge reveals expression in ECs. (B) Higher-resolution imaging localizes Sema3d expression inside the leading edge ECs at 30 hpf (white arrowheads). (C) Model of the two Sema3d expression domains (magenta, Sema3d; green, ECs).

localization. Antibody staining revealed that Sema3d is localized in the mesenchyme next to the CCV at 25 and 32 hpf (Fig. 2 A). At 32 hpf, Sema3d was additionally expressed in the ECs of the CCV leading edge. By confocal imaging, we clearly visualized the anti-Sema3d signal in vesicles inside the green *kdrl:GFP*-positive cells of the CCV leading edge cells (Fig. 2, A and B). *sema3d* morphants and mutants completely lacked Sema3d staining (Fig. S1 E). By in situ hybridization, we confirmed the *sema3d* expression from the mesenchyme and the leading edge ECs (Fig. S2 C). Likewise, *Sema3d* expression by ECs has been shown in human umbilical vein ECs (HUVECs; Serini et al., 2003). Overall, we showed that there are two distinct *sema3d* expression domains (Fig. 2 C): *sema3d* is expressed in the mesenchyme on both sides of the CCV and in the ECs of the CCV leading edge.

Mesenchymal Sema3d acts as a repulsive cue for CCV outgrowth

Sema3d has been shown to act as a repulsive cue during axon guidance (Liu et al., 2004; Wolman et al., 2004). To figure out whether Sema3d mediates CCV repulsion, we performed global *sema3d* overexpression with *sema3d* mRNA injection (Fig. 3 A) or *sema3d* overexpression upon heat shock in the transgenic line *Tg(hsp70:sema3dGFP)* (Fig. 3 B). Overexpression did not abolish outgrowth completely, but CCV width was significantly reduced by one third (from 120 to 80 µm; Fig. 3 C). We hypothesized that mesenchymal Sema3d acts as a repulsive cue on CCV collective migration. To test this, we performed mosaic *sema3d* knockdown through injection of *sema3d* MO together with DiI for cell tracking into 1 of 16 cells (Fig. 3 D). Partial loss of *sema3d* in the mesenchyme next to the CCV induced ECs to migrate into the mesenchyme area. This indicates that the bilateral mesenchymal *sema3d* expression domains provide Sema3d as a repulsive cue to direct medial CCV outgrowth.

EC-specific Sema3d is required for EC sheet organization and collective migration

At 24 hpf, the CCV is an open-ended cylinder (Fig. 1 B), located between the two mesenchymal *sema3d* expression domains (Fig. 2 A). From the roof of the cylinder, the ECs migrate ventrally as a cell sheet underneath the epidermis. At 30 hpf, no other tissue is located in proximity of the extended cell sheet (Fig. S4 C). Based on EC-specific *sema3d* expression in the leading edge (Fig. 2 and Fig. S2 C), we hypothesized that the *sema3d* knockdown phenotype in the CCV leading edge depends on EC-specific Sema3d. Therefore we aimed to delete *sema3d* selectively in the CCV leading edge ECs by two different approaches: time-specific *sema3d* photo-MO activation (Fig. 4) and mosaic *sema3d* knockdown through injection of MO in only one of 16 blastomeres (Fig. S4).

We used light-inducible cleavage of an inhibiting sense (SE)–MO to specifically activate the *sema3d* antisense (AS)-MO at chosen time points. For this approach, the *sema3d* AS-MO was injected in combination with a pairing *sema3d* SE-photo-MO, resulting in an inactive, bound MO pair (called AS+SE-photo-MO). UV light–induced cleavage of the SE-MO destroys the pairing and thereby frees the *sema3d* AS-MO to bind to *sema3d* mRNA and inhibit protein translation. In short, the *sema3d* MO is active only after UV induction (Fig. 4 A). We showed that UV exposure itself had no effect on Ctr MO-injected embryos in terms of CCV width and cell sheet morphology (Fig. 4, B–C′). Likewise, SE-photo-MO–injected embryos that were not exposed to UV light showed a WT phenotype, similar to Ctr MO-injected embryos (Fig. 4, E and E′). To control whether UV light exposure of AS+SE-photo-MO indeed reproduces the phenotype obtained by *sema3d* MO injection, we exposed whole AS+SE-photo-MO–injected embryos to UV light at 9 hpf (Fig. 4, F and F′). Indeed, MO activation at 9 hpf completely reproduced the phenotypes observed in Sema3d-deficient embryos and induced wider CCVs and disrupted cell sheet morphology as in *sema3d* morphants and mutants

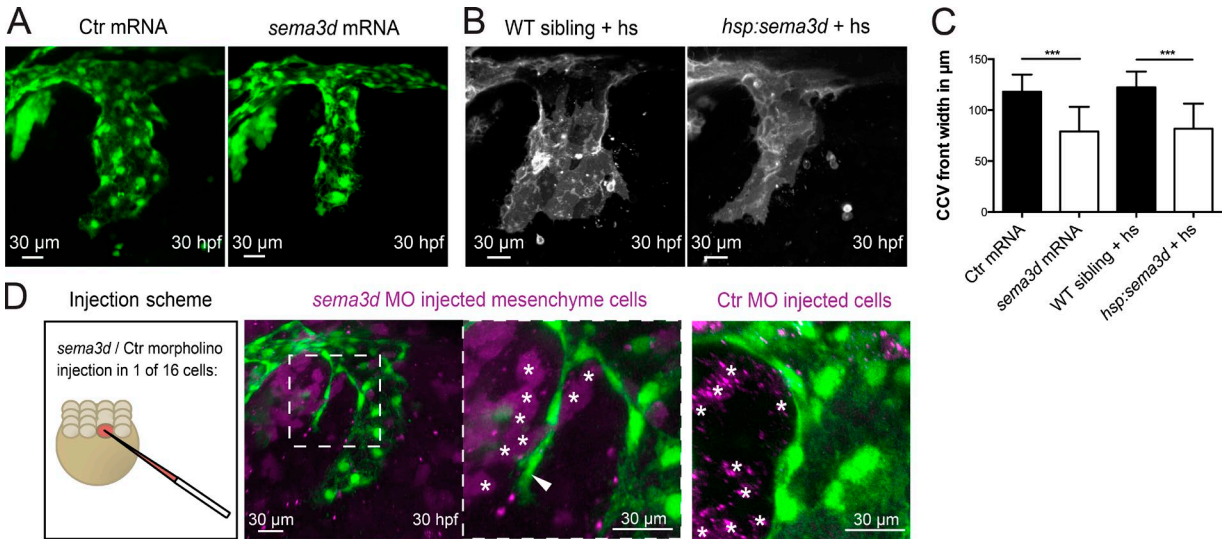

Figure 3. **Mesenchymal Sema3d acts as a repulsive cue for CCV outgrowth.** (A–C) Global *sema3d* overexpression reduces CCV width. (A) *sema3d* mRNA–injected *Tg(kdrl:EGFP)*^{s843} embryos exhibit reduced CCV width at 30 hpf. (B) *sema3d* expression was induced by consecutive heat shocks (hs) at 16 and 19 hpf (each for 1 h at 39°C) in *Tg(hsp70:sema3dGFP)*, *Tg(kdrl:HRAS-mCherry)*^{s896} embryos. *sema3d*-overexpressing embryos show a thinner CCV at 30 hpf. (C) Quantification of CCV front width (each $n = 18$). Error bars indicate SD. (D) Mosaic *sema3d* k.d. through *sema3d* MO injection into one of 16 cells in *Tg(kdrl:EGFP)*^{s843} embryos (magenta, coinjection with DiI for cell tracking). Partial loss of *sema3d* in the mesenchyme (white asterisks) induced ECs (white arrowhead) to migrate into the mesenchyme ($n = 3$), indicating that *sema3d* acts as a repulsive cue in the mesenchyme next to the CCV. Ctr MO-injected mesenchymal cells (white asterisks in right panel) did not induce ectopic EC migration. ***, $P < 0.001$.

(Fig. 4 B, compare with Fig. 1, E and F; and Fig. 4, compare F and F′ with D and D′).

Next, we chose to activate the *sema3d* MO and thereby stop Sema3d protein production at different time points of CCV development. At 24 hpf, the CCVs formed between the two mesenchymal *sema3d* expression domains, but did not extend beyond them. UV exposure at 24 hpf resulted in a mean CCV width of 173 µm (Fig. 4, B and G) and therefore affected the CCV width much less severely than UV-mediated induction at 9 hpf (207 µm; Fig. 4, B and F), although CCVs were still wider than Ctr CCVs (125 µm; Fig. 4, B and E). In contrast, the CCV leading edge still exhibited disrupted cell morphology and reduced cell–cell junctions (Fig. 4 G′).

To investigate the effect of Sema3d loss after the CCV cell sheet has extended beyond the mesenchymal *sema3d* expression domains, and therefore to target only the EC-specific *sema3d* expression in this region, we exposed AS+SE-photo-MO–injected embryos to UV light at 27 hpf (Fig. 4, B, H, and H′). These embryos exhibited a CCV of normal width but still showed the full phenotype of disrupted cell morphology and reduced cell–cell contacts in the leading edge ECs.

As a second approach to perform *sema3d* knockdown in the CCV leading edge ECs, we injected *sema3d* MO into one of 16 blastomeres (Fig. S4 A). Thereby, we randomly targeted different cell populations with the *sema3d* MO (tracked by coinjected DiI). In a few cases, we targeted only CCV ECs in this region (four of 200). These CCVs exhibited the described leading edge phenotype of a disrupted cell sheet with lesions (Fig. S4, A and B). Targeting mesenchymal cells, blood cells, or epidermal cells did not induce any changes in the leading edge (Fig. S4 B).

Both time-specific *sema3d* photo-MO activation and EC-specific Sema3d depletion showed that Sema3d signaling induced lesions in the EC sheet, most probably via an autocrine mechanism. In sum, our experiments indicate that EC-specific Sema3d acts independently of mesenchymal Sema3d and is required for EC sheet organization and collective migration.

Sema3d regulates Actin network organization in leading edge ECs controlling cell shape and contacts

In addition to the described lesions in the CCV front in *sema3d* morphants and mutants, ECs also exhibit impaired cell morphology (Figs. 1 F and 5 A). To assess changes in morphology, we measured the cell shape factor, with a value of 1 indicating a perfectly round shape (Fig. 5 B). Whereas Ctr MO-injected cells had a cell shape factor of 0.7, Sema3d-deficient cells had a mean cell shape factor of 0.4, confirming that Sema3d regulates cell morphology directly or indirectly at the leading front of the CCV migrating cell sheet (Fig. 5 B).

We hypothesized that loss of Sema3d could alter the Actin cytoskeleton of leading edge ECs or act on EC junctions. Therefore, we first investigated the cellular Actin structure by imaging of *Tg(fli1a:lifeactEGFP)*^{mu240} embryos. In *sema3d* morphants and mutants the cohesive cell sheet was disrupted and cells lacked cell–cell contacts (Fig. 5 A). Live imaging illustrated the inability of *sema3d* morphant ECs to form a consistent cell sheet (Ctr MO in Video 3 vs. *sema3d* morphant in Video 4). Moreover, in Ctr MO and WT siblings Actin cables were arranged in parallel to the leading front. These organized Actin cables were not present in Sema3d-deficient cells (Fig. 5, A and E). To analyze whether partial impairment of Actin polymerization is sufficient to cause the observed phenotype, we inhibited Actin/Myosin polymerization by applying blebbistatin or latrunculin A from 22 to 30 hpf. Interestingly, inhibition of Actin/Myosin polymerization completely phenocopied the disrupted CCV sheet morphology that we observed in *sema3d* mutants, but did not lead to a wider CCV (Fig. 5 C). Analysis of this experiment with *Tg(fli1a:lifeactEGFP)*^{mu240} embryos was not possible, as inhibition of Actin polymerization prevents incorporation of the fluorescent F-Actin fragments of the Lifeact reporter.

To elucidate the mechanism by which Sema3d regulates Actin network organization, we investigated potential Sema3d

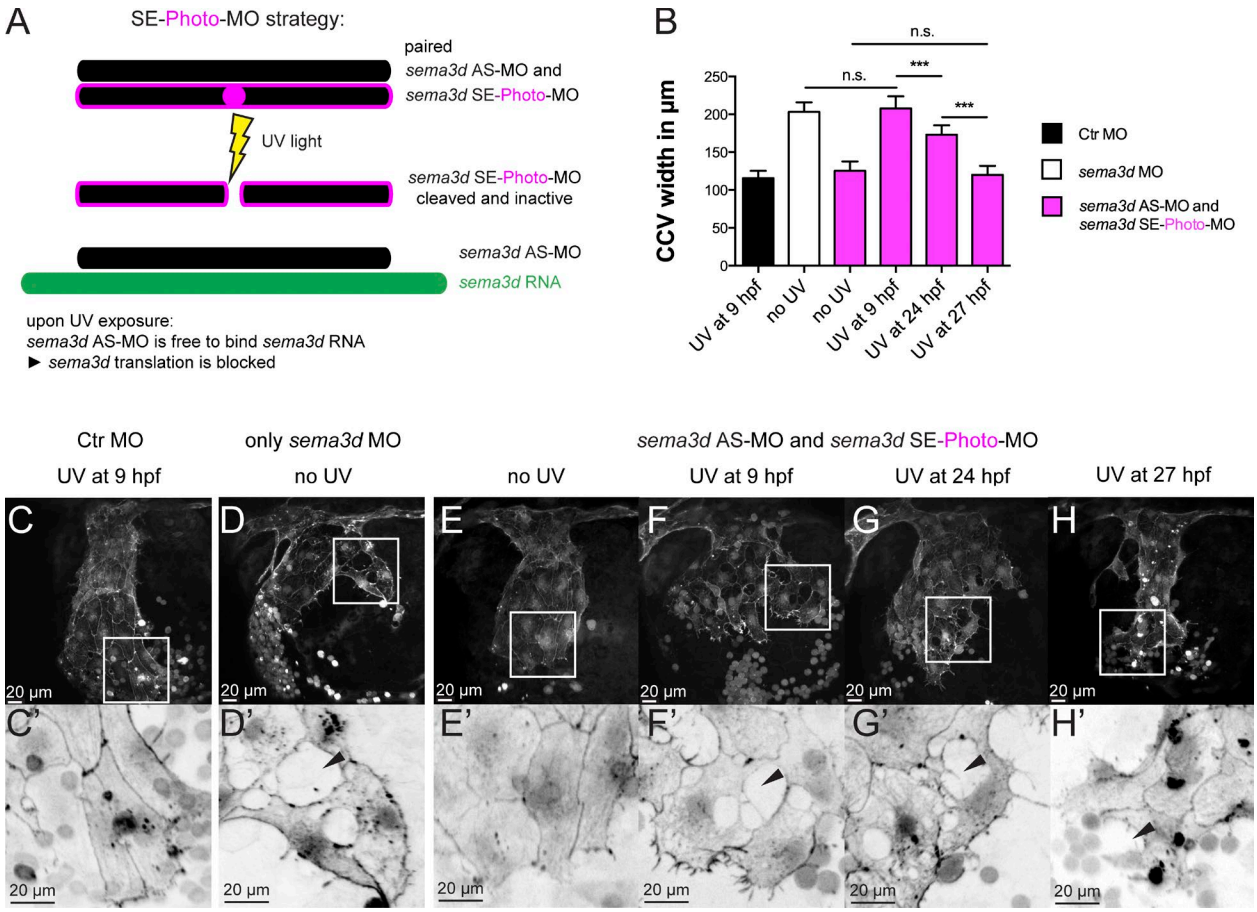

Figure 4. **EC-specific Sema3d acts independently of mesenchymal Sema3d and is required for EC sheet organization and collective migration.** Time-specific *sema3d* knockdown with photo-MOs suggests that EC-specific Sema3d is capable of preserving a cohesive EC sheet. (A) SE-photo-MO strategy for time-specific *sema3d* knockdown consists of the *sema3d* AS-MO, paired to a UV light–cleavable *sema3d* SE-photo-MO (together called AS+SE-photo-MO). UV light induces cleavage of the *sema3d* SE-photo-MO, enabling the *sema3d* AS-MO to bind *sema3d* mRNA and block translation at a chosen time point. (B–H′) *Tg(fli1a:lifeactEGFP)*^{mu240} embryos injected with Ctr MO (C), *sema3d* MO (D), or AS+SE-photo-MO (E–H) were exposed to UV light at the indicated time points and analyzed at 30 hpf. (B) Quantification of CCV front width (each $n = 10$). ***, $P < 0.001$; n.s., not significant. Error bars indicate SD. (C and C′) UV exposure has no effect on Ctr MO-injected embryos. (D) *sema3d* morphants show typical phenotype of widened CCV with lesions in the leading edge (black arrowhead). (E and E′) Without UV induction, the AS+SE-photo-MO–injected embryos resemble Ctr MO. (F and F′) UV activation of AS+SE-photo-MO–injected embryos at 9 hpf results in the *sema3d* MO phenotype (compare with D and D′). (G and G′) After UV exposure at 24 hpf, AS+SE-photo-MO–injected embryos exhibit an intermediate CCV width (compare with F) but disrupted cell–cell contacts (black arrowhead). (H and H′) AS+SE-photo-MO–injected embryos, exposed to UV light at 27 hpf, exhibit a CCV of normal width (compare with F) but disrupted cell–cell contacts in the front (black arrowhead).

downstream effectors. Class III Semaphorins and their receptors have been shown to interact with multiple GTPases (Püschel, 2007). The GTPases RhoA, Rac1, and Cdc42 have been linked to regulation of Actin cytoskeleton organization (Sit and Manser, 2011). We used pharmacological inhibitors against each of these GTPases from 22 to 30 hpf and analyzed Actin cable formation and cell–cell contacts in *Tg(fli1a:lifeactEGFP)*^{mu240} embryos. We showed that Rac1 and Cdc42 are not involved in the regulation of CCV collective cell migration (Fig. 5, D and F).

However, inhibition of either RhoA or its downstream effector Rock induced the same leading edge phenotype as Sema3d depletion, characterized by lesions in the cell sheet as well as a loss of intracellular parallel Actin cables (Fig. 5 F). To quantify the CCV cell–cell contact phenotype, we determined the distance of cell–cell contacts per cell in relation to the perimeter (Fig. 5 D). Free cell edges such as the leading front, which cannot make any cell contact, were added to the cell–cell contact length. Because of the variable size of leading-front lengths, the minimum percentage of cell–cell contacts would therefore be roughly 20%. Ctr cells exhibited ∼100% of perimeter with cell–cell contacts, whereas this number was reduced to 65–69% in *sema3d* morphants and mutants as well as in RhoA or Rock inhibitor–treated embryos (Fig. 5 D). Accordingly, the percentage of CCV front cells with aligned Actin cables was also reduced by at least 75% upon knockdown of *sema3d* and inhibition of RhoA or Rock (Fig. 5, E and F).

Additionally, it has been shown that FAK can control Actin assembly (Serrels et al., 2007). We therefore also investigated the contribution of FAK to the phenotype. Inhibition of FAK resulted in loss of Actin cables but not of cell–cell contacts (Fig. 5, D–F). We conclude that Actin cable assembly can depend on FAK; however, formation of the cohesive cell sheet and CCV migration seemed to be independent of FAK. Taken together, these experiments indicate that Sema3d regulates cell–cell contact formation and Actin assembly in ECs through the effector kinases RhoA and Rock.

Interestingly, we observed a comparable function of Sema3d in mediating cell–cell contacts in Ses. As noted

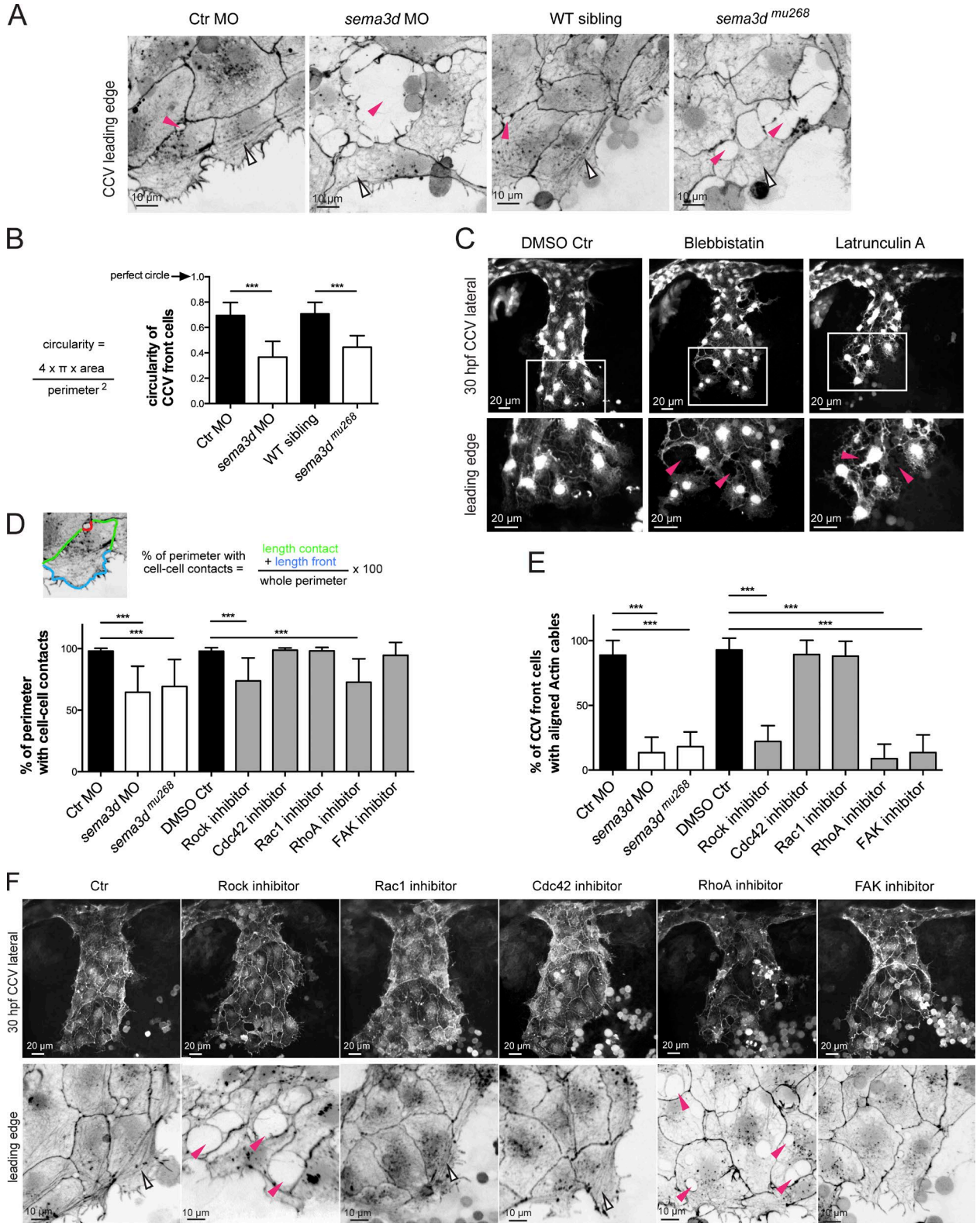

Figure 5. **Sema3d acts on Actin network organization in leading edge ECs controlling Actin cable formation, cell shape, and contacts.** (A) The cohesive cell sheet in the CCV leading edge is disrupted and exhibits lesions (pink arrowheads) in *sema3d* morphants and mutants at 30 hpf. In Ctr embryos, Actin cables are arranged parallel to the leading front; they are absent in Sema3d-deficient embryos (open arrowheads). High-resolution confocal projections of *Tg(fli1a:lifeactEGFP)*^{mu240} embryos from Fig. 1 F were color-inverted. (B) Quantification of the circularity of CCV leading edge cells illustrates that loss of *sema3d* significantly alters cell shape (each $n = 24$). (C) Inhibition of Myosin/Actin phenocopies *sema3d* phenotype of disrupted cell–cell contacts (pink arrowheads) but does not lead to a wider CCV. Confocal projections of *Tg(kdrl:EGFP)*^{s843} embryos at 30 hpf. (D) The length of cell perimeter with cell–cell contacts of CCV leading edge cells is reduced in *sema3d* morphants and mutants and after Rock or RhoA inhibition. Inhibition of Rac1, Cdc42, or FAK had no effect on cell–cell contacts ($n = 30$ for morphants and mutant cells and $n = 18$ for inhibitor experiments). (E) Quantification of front cells with aligned

earlier, Ses were stalled at the horizontal myoseptum because of migrational defects in Sema3d-deficient embryos (Fig. S3, A–C). To elucidate the effect of EC-specific *sema3d* knockdown, we transplanted *sema3d* MO-injected *Tg(kdrl:EGFP)*^{s843} donor cells into WT *Tg(kdrl:HRAS-mCherry)*^{s896} hosts and analyzed the vascular defects (Fig. S3 D). In the case of global *sema3d* knockdown or transplanted Sema3d-deficient muscle tissue, Ses were stalled at the horizontal myoseptum (Fig. S3 E). In the case of EC-specific knockdown, Se cells lost their connections to neighboring cells (Fig. S3 F). We conclude that EC-specific Sema3d is required for cell–cell contact formation in Ses and for Se cell migration (Fig. S3 G).

Next, we analyzed the contribution of cell–cell junctions to the regulation of EC migration. We hypothesized that loss of cell–cell contacts could be caused by a misregulation of junctional proteins. Previously, we showed that loss of the adherens junction molecule Cdh5 impairs the directional migration of CCV cells (Helker et al., 2013). Interestingly, we observed a similar effect on directional EC migration in *sema3d* mutants and morphants (Fig. 1, I and J). To determine whether misregulation of Cdh5 downstream of Sema3d impairs directionality, we analyzed *cdh5* expression. *cdh5* mRNA expression was not altered in *sema3d* mutants and morphants (Fig. S2, E and F). Additionally, we analyzed Cdh5 protein distribution together with the tight junction molecule zonula occludens 1 (ZO-1; Fig. 6 A). *sema3d* morphant ECs exhibited altered distribution of junctional proteins: although ZO-1 staining was equally distributed at the cell edges, Cdh5 staining was aberrantly distributed in a patchy pattern and lost in several locations. We quantified the total length of Cdh5-positive cell perimeter in relation to the whole perimeter and found it to be reduced by more than 20% in Sema3d-deficient cells (Fig. 6 B). However, when analyzing cell–cell contact length using *Tg(fli1a:lifeactEGFP)*^{mu240} embryos, we found no changes in *cdh5* mutants (Fig. 6, C and E). Interestingly, Cdh5-deficient CCV ECs exhibited tiny holes within the ECs themselves (Fig. 6 C, pink arrowheads). We speculate that these holes within the cells might contribute to a loss of cell sheet tension, much as the reduction in cell–cell contacts upon Sema3d deficiency might lead to the described phenotype of impaired directional migration. To exclude direct regulation of cell–cell contacts by blood flow, we inhibited flow with nifedipine and tricaine from 22 to 30 hpf. We observed no change in cell–cell contact length under these conditions (Fig. 6, D and E).

Taken together, our experiments reveal that *sema3d* knockdown alters the distribution of junctional proteins and affects the cytoskeleton, resulting in an impaired EC shape as well as a loss of cell–cell contacts and Actin cables. We conclude that EC-specific Sema3d regulates Actin polymerization via RhoA and Rock in leading edge ECs independently of Cdh5 and flow.

The differential functions of Sema3d are transduced by different receptors

We have shown that on the one hand Sema3d acts as a repulsive cue and on the other hand as a regulator of Actin network organization facilitating a consistent cell sheet organization. Therefore, we asked how the same molecule could act on the same EC population but elicit very different phenotypic responses. One hypothesis is that the different responses are mediated by signaling through different Sema3d receptors. Class III Semaphorin proteins are secreted ligands and have been reported to signal through class A and D Plexins and Neuropilin 1 and 2 (Gu and Giraudo, 2013). Therefore, we used in situ hybridization to investigate the expression pattern of all potential Sema3d receptor candidates: *plxnA1b*, *plxnA2*, *plxnA3*, *plxnD1*, *nrp1a*, *nrp1b*, *nrp2a*, and *nrp2b*. Of these only *plxnD1*, *nrp1a*, and *nrp1b* were expressed in the CCV (Fig. 7 A). *cdh5* was used as a control, as it labels all CCV ECs. In comparison to *cdh5*, *plxnD1* was specifically expressed in the most dorsal CCV ECs. In contrast, *nrp1a* was expressed within the whole CCV, including the leading edge.

To analyze whether the differential roles of Sema3d are mediated by differential receptor signaling, we analyzed PlxnD1- or Nrp1-deficient embryos. MO-mediated loss of *plxnD1* led to an increased CCV width (Fig. 7 B). Ctr MO-injected embryos exhibited a CCV width of ∼120 µm, whereas *plxnD1* MO-injected embryos had CCV widths of ∼200 µm (Fig. 7 D). Indeed, loss of *plxnD1* phenocopied the increased CCV width phenotype of *sema3d* morphants and mutants (Fig. 1, compare E and H). However, analysis of the CCV leading edge cell sheet did not show any disruption of the cohesive EC sheet (Fig. 7 B). Measurement of the percentage of cell perimeter with cell–cell contacts showed no significant difference between *plxnD1* morphants and Ctr morphants (Fig. 7 G).

In contrast, *nrp1a*^{hu10012} mutant embryos and *nrp1a/b* morphants did not show an increased CCV width (Fig. 7, C, D, and F). Nevertheless, the CCV leading edge exhibited a disorganized cell sheet with an increased number of lesions in *Tg(kdrl:EGFP)*^{s843}-positive *nrp1a*^{hu10012} mutant embryos (Fig. 7 E). The increased number of lesions could also be observed by measuring the cell–cell contact length in relation to the perimeter in *Tg(fli1a:lifeactEGFP)*^{mu240}-positive *nrp1a/b* and *nrp1a* morphants (Fig. 7, F and G). Whereas Ctr morphant cells exhibited 98% of perimeter with cell–cell contacts, this number was reduced to 73% in *nrp1a/b* morphants and 83% in *nrp1a* morphants (Fig. 7 G).

In summary, loss of Sema3d results in a wide CCV with lesions, *plxnD1* knockdown in a wide CCV only, and *nrp1* knockdown in a disrupted cell sheet with lesions (Fig. 7 H). Nrp1 is localized in the whole CCV and especially in the leading edge ECs, whereas PlxnD1 is localized only in the upper CCV (Fig. 7 I).

Plxn receptor activation always occurs downstream of Sema binding (Janssen et al., 2010), but Nrp is a multifunctional coreceptor that can be activated by different ligands and act in complex with different receptors (Pellet-Many et al., 2008). We specifically addressed the involvement of Vegf and Vegf receptor (VegfR) in the regulation of CCV collective migration (Fig. S5). Although our data did not support involvement of VegfA ligands, we could not resolve whether VegfR acts as a Nrp1 coreceptor in the context of EC migration (Fig. S5, A–D). However, we could clearly show that Sema binding to Nrp1 is required for regulating Actin cable and cell–cell contact formation, as Nrp1

Actin cables (n = 10 for morphants or mutants and n = 7 for inhibitor experiments). (F) Lateral confocal projections of *Tg(fli1a:lifeactEGFP)*^{mu240} embryos at 30 hpf. Leading edge high magnifications were color-inverted. Inhibition of Rock and RhoA induced lesions in the leading edge (pink arrowheads). Parallel-arranged Actin cables (open arrowheads) are missing after inhibition of Rock, RhoA, or FAK. ***, P < 0.001. Error bars indicate SD.

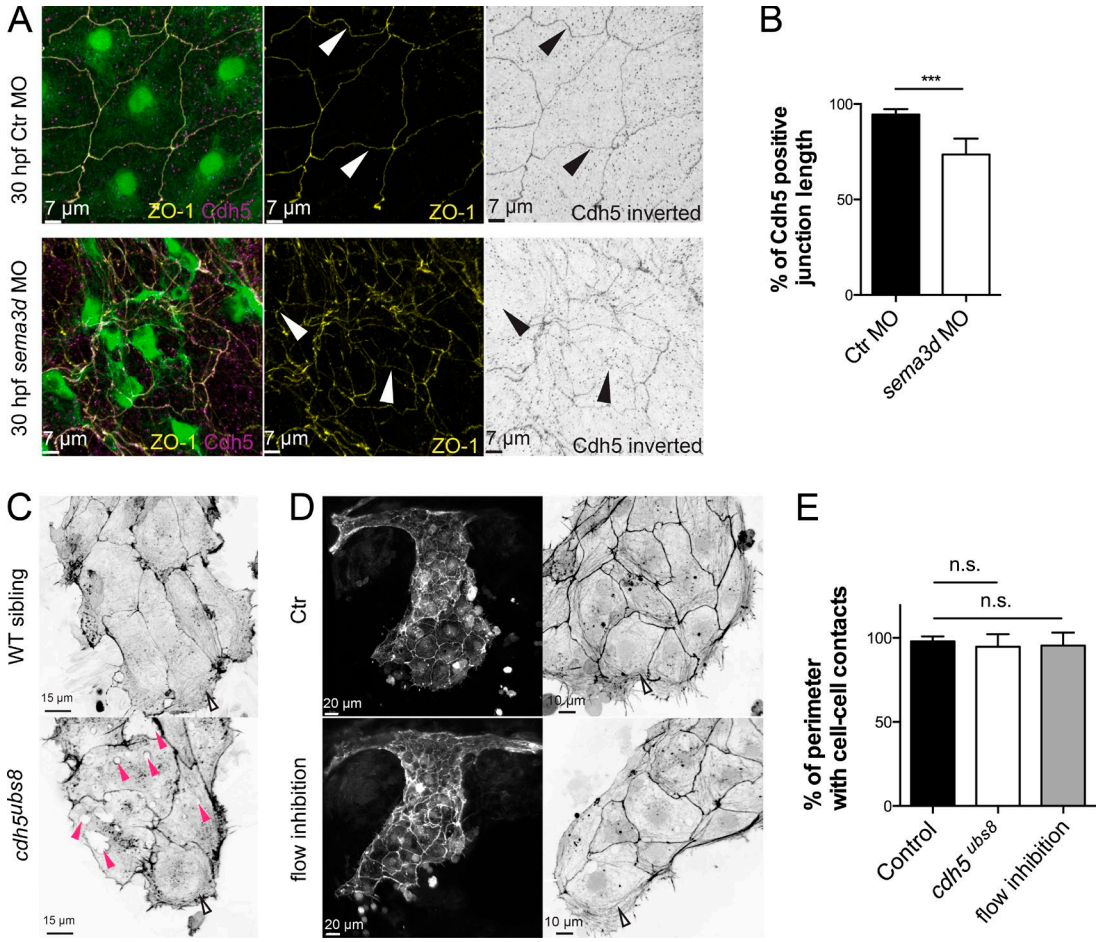

Figure 6. **Loss of cell–cell contacts in the CCV leading edge did not depend on flow or Cdh5.** (A) Antibody staining for ZO-1 and Cdh5 showed aberrant junction distribution and impaired cell shape upon *sema3d* loss. Arrowheads indicate gaps in Cdh5 protein distribution. (B) The length of Cdh5-positive cell–cell connections is reduced in *sema3d* morphants ($n = 4$). (C) Cell–cell connections in the CCV leading edge of *cdh5*^{ubs8} mutant embryos are present, but the ECs exhibit holes inside the cells (pink arrowheads). (D) Flow inhibition with nifedipine and tricaine did not lead to lesions or impaired Actin cable alignment in the CCV leading edge. Parallel-arranged Actin cables are indicated by open arrowheads. (E) Quantification of cell–cell-contact length of CCV leading edge cells ($n = 16$). ***, $P < 0.001$; n.s., not significant. Error bars indicate SD.

protein variants lacking the Sema3d binding domain (Nrp1Δa) could not rescue Nrp1 deficiency (Fig. S5, E–H). To summarize, we propose that mesenchymal Sema3d signals through PlxnD1 via repulsion inducing a straight CCV outgrowth, whereas EC-specific Sema3d signals through Nrp1 via RhoA and Rock and facilitates coherent cell sheet organization.

Sema3d-Nrp1 signaling regulates cell–cell contacts and Actin cable formation in the CCV leading edge by activating RhoA

To investigate whether RhoA- and Rock-mediated Actin network organization in the CCV leading edge acts downstream of Sema3d-Nrp1 signaling, we performed rescue experiments using pharmacological activation of RhoA (Fig. 8). Untreated *Tg(fli1a:lifeactEGFP)*^{mu240} Sema3d-deficient embryos as well as *nrp1a/b* morphants exhibited lesions in the leading edge and had few cells with Actin cables (Fig. 8 A). RhoA activation in these morphants and mutants from 22 to 30 hpf rescued cell–cell contact formation in the CCV cell sheet and restored the formation of Actin cables (Fig. 8, B and C). RhoA activation increased cell–cell contact length in Sema3d-deficient and *nrp1a/b* morphant embryos by 19% and 17%, respectively (Fig. 8 C). Similarly, RhoA activation restored the percentage of CCV front cells with aligned Actin cables from 15% to 87% in *sema3d* morphants, from 19% to 80% in *sema3d* mutants, and from 22% to 87% in *nrp1a/b* morphants (Fig. 8 D). Interestingly, the increase of CCV width seen in *sema3d* morphants and mutants was not normalized by RhoA activation. Taken together, our data show that Sema3d-Nrp1 signaling regulates cell–cell contacts and Actin cable formation in the CCV leading edge though RhoA activation.

Sema3d directly regulates collective cell migration

Based on Sema3d localization in the mesenchyme next to the CCV as well as in the leading edge ECs, we propose two mechanisms of Sema3d regulating collective migration in vascular development. On the one hand, mesenchymal Sema3d signals in a paracrine fashion through PlxnD1 via repulsion and induces straight CCV outgrowth; on the other hand, EC-specific Sema3d signals in an autocrine fashion through Nrp1 via RhoA and Rock and facilitates consistent cell sheet organization and migration through affecting cell–cell contact and Actin cable formation (Fig. 9).

Hereby we demonstrate that Sema3d is a novel regulator of collective EC migration. Class III Semaphorins have so far

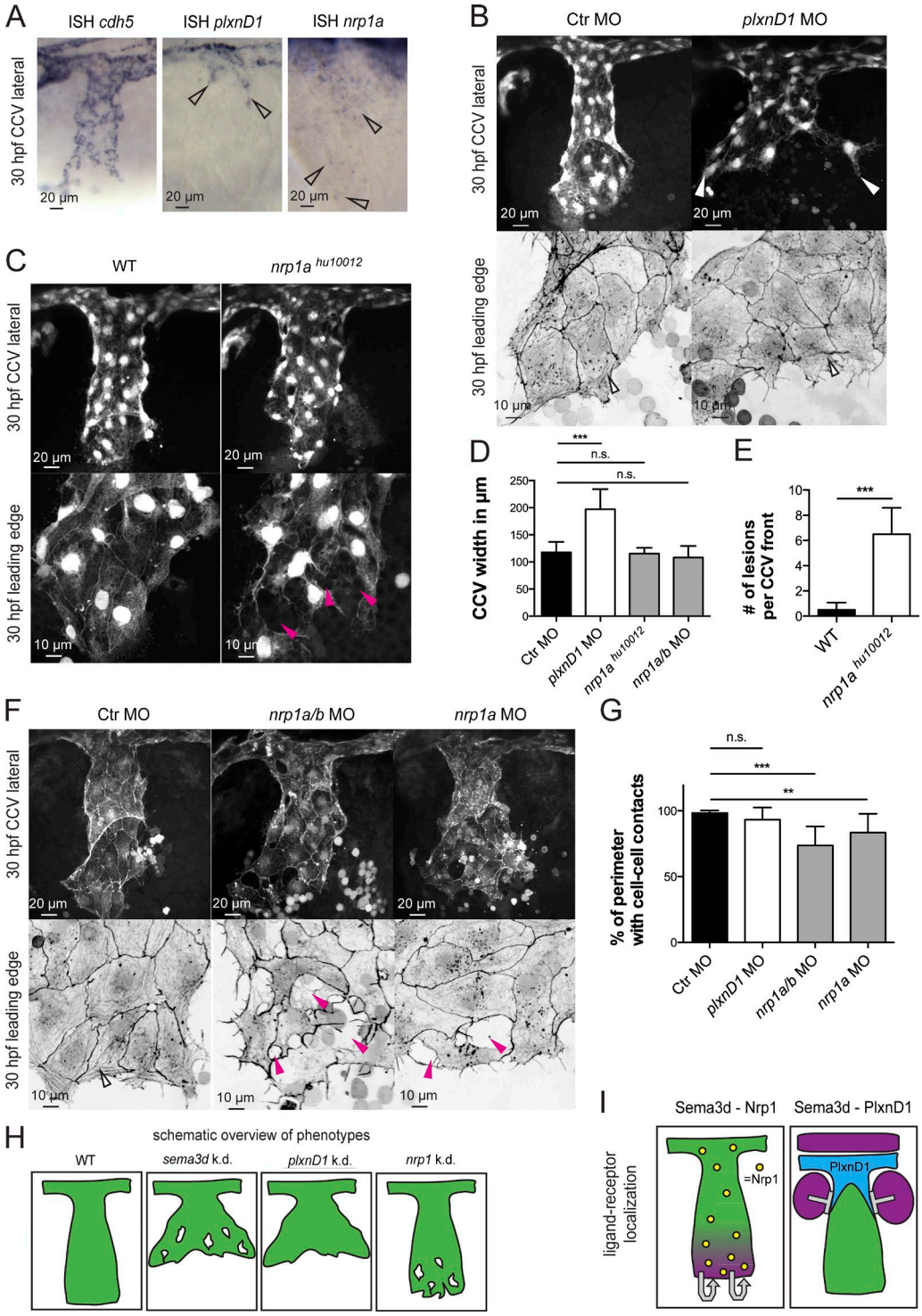

Figure 7. **Differential Sema3d functions are transduced by signaling through the different receptors Nrp1 or PlxnD1.** (A) In situ hybridization (ISH) of 30-hpf embryos showing *cdh5* expression in all CCV cells, *plxnD1* expression in the dorsal-most CCV cells (open arrowheads), and *nrp1* expression in all CCV cells (open arrowheads). (B–G) Analysis of PlxnD1 or Nrp1 deficiency in *Tg(kdrl:EGFP)*^{s843} or *Tg(fli1a:lifeactEGFP)*^{mu240} embryos at 30 hpf. (B) Loss of PlxnD1 led to a wider CCV (white arrowheads), but cell–cell contacts were not impaired, and parallel-arranged Actin cables were present (open arrowheads). (C) *nrp1a*^{hu10012} mutant embryos had reduced cell–cell contacts (pink arrowheads) but did not exhibit a wider CCV. (D) Quantification of CCV front width (each $n = 11$; *nrp1a*^{hu10012}, $n = 4$). (E) Number of lesions in *nrp1a*^{hu10012} mutant embryos is increased compared with WT ($n = 4$). (F) *nrp1a/b* and *nrp1a* morphant CCVs exhibit a normal width, but the leading edges showed lesions (pink arrowheads) and lacked Actin cables (compare with open arrowhead in Ctr). (G) Quantification of cell–cell contact length (each $n = 13$). (H) Schematic overview of phenotypes comparing Sema3d deficiency with *plxnD1* and *nrp1* knockdown. (I) Schematic illustration of ligand-receptor localization indicating autocrine Sema3d-Nrp1 signaling and paracrine Sema3d-PlxnD1 signaling. Magenta, *sema3d* expression; green, CCV ECs; blue, *plxnD1* expression; and yellow, *nrp1* expression. ***, $P < 0.001$; **, $P < 0.01$; n.s., not significant. Error bars indicate SD.

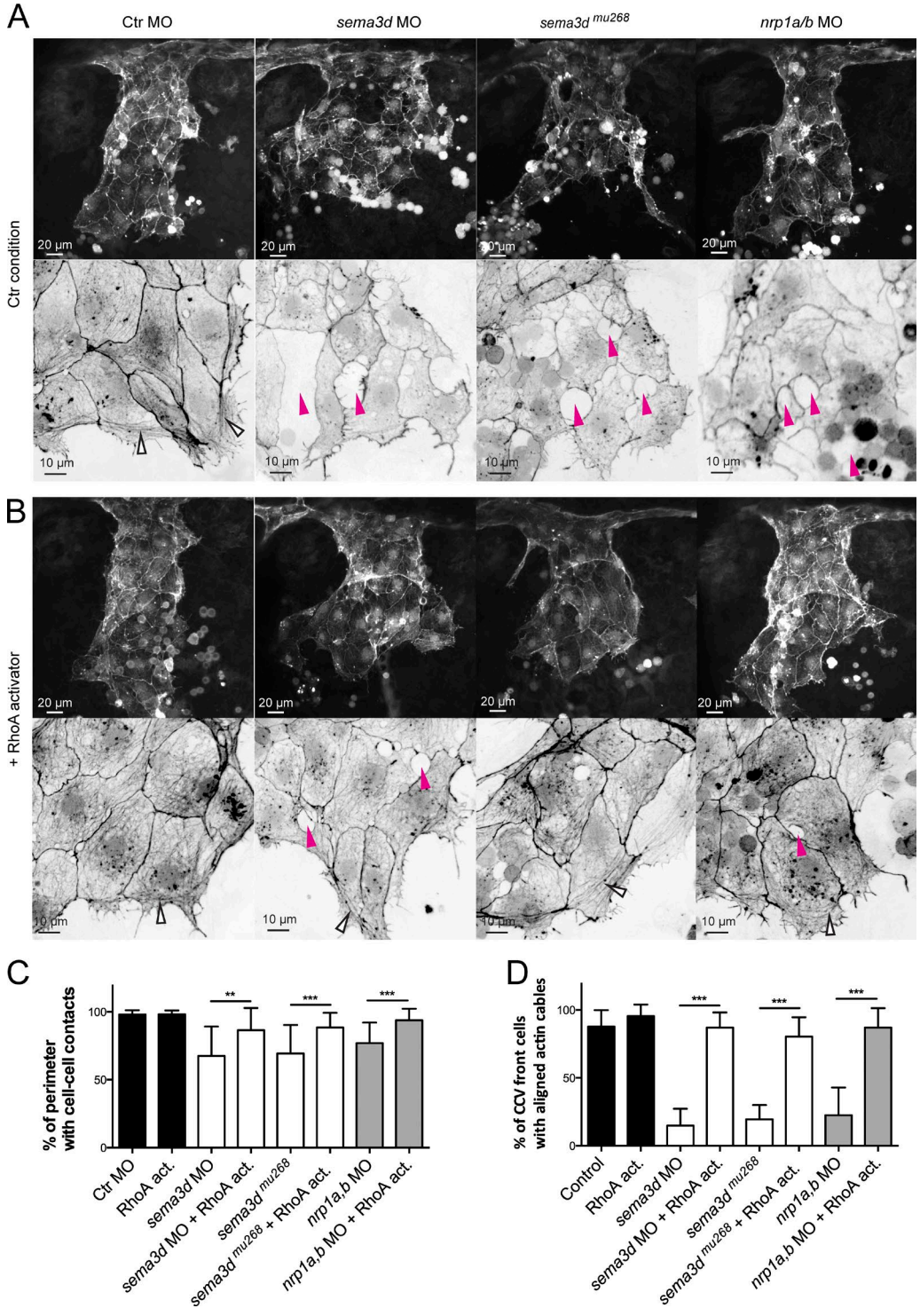

Figure 8. **Sema3d-Nrp1 signaling regulates cell–cell contacts and Actin cable formation in the CCV leading edge by activating RhoA.** (A and B) Lateral confocal projections of *Tg(fli1a:lifeactEGFP)*^{mu240} embryos at 30 hpf. Magnifications of the leading edges were color-inverted. (A) *sema3d* morphants and mutants as well as *nrp1a/b* morphants exhibited lesions in the leading edge (pink arrowheads) and lacked parallel-arranged Actin cables (open arrowhead in Ctr MO). (B) Activation of RhoA from 24 to 30 hpf reduced lesions (pink arrowheads) and rescued Actin cable formation (open arrowheads) in *sema3d* morphants and mutants as well as in *nrp1a/b* morphants. (C and D) Quantification of cell–cell contact length (C, $n = 16$) and cells with Actin cables (D, each $n = 8$; *sema3d*^{mu268} + RhoA activator, $n = 4$). ***, $P < 0.001$; **, $P < 0.01$. Error bars indicate SD.

been reported only for guiding neural crest cell streams via a repulsive mechanism (Eickholt et al., 1999; Yu and Moens, 2005; Gammill et al., 2007). Additionally, Sato et al. (2006) reported that in the cardiac neural crest, knockdown of *sema3d* results in impairment of migration, but the mechanism of action was not elucidated. To analyze whether Sema3d might regulate collective cell migration of other tissues, we investigated collective cell migration of the zebrafish lateral line primordium (LLP).

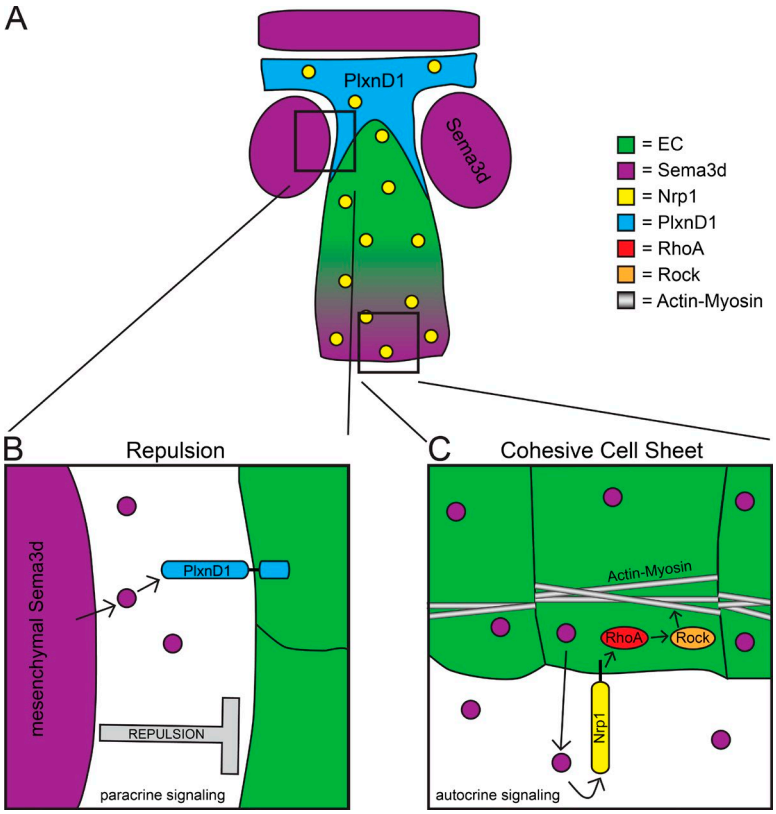

Figure 9. **Sema3d controls collective EC migration via repulsion and regulation of Actin network organization, mediating a cohesive cell sheet.** (A) Schematic overview of ligand-receptor localization in the CCV. Sema3d (magenta) is localized in the mesenchyme next to the CCV and in the CCV leading edge. PlxnD1 (blue) is localized in the dorsal part of the CCV. Nrp1 (yellow) is localized in the whole CCV. Seam3d regulates collective EC migration via repulsion (B) and regulation of Actin network organization controlling cell sheet organization (C). (B) Sema3d is secreted from the mesenchyme and mediates repulsion on ECs via the EC-specific receptor PlxnD1 in a paracrine manner. Thus, Sema3d mediates straight outgrowth of the CCVs. (C) In contrast, EC-specific Sema3d in the leading edge regulates cell migration by autocrine signaling through Nrp1. Sema3d-Nrp1 signaling mediates Actin network organization via RhoA (red) and Rock (orange) regulating cell shape, cell–cell contacts, and Actin cable formation.

We showed by antibody staining and in situ hybridization that Sema3d is expressed in the LLP and its deposited neuromasts (Fig. 10 A). Upon *sema3d* knockdown, LLP migration distance was reduced and rosette organization was impaired (Fig. 10, B–D). The observed phenotype of reduced migration and impaired cellular organization resembles the phenotype observed in CCV ECs, illustrating the importance of Sema3d in regulating collective cell migration in other developmental contexts.

Discussion

Our work reveals two separate roles of Sema3d for the regulation of collective EC migration. Spatiotemporally regulated Sema3d expression in combination with signal transduction through different receptors induces the differential functions of Sema3d-mediated repulsion of ECs on the one hand and migration of these ECs on the other hand (Fig. 9). This is the first study to elucidate the mechanisms by which Sema3d fulfills these contrary functions in vivo.

We show that mesenchymal Sema3d controls straight and directional migration of ECs, most likely by repulsion through the EC-specific receptor PlxnD1, in a paracrine manner (Fig. 9 B). Thereby Sema3d guides the migration route of the ECs and supports collective migration. PLXND1 was previously shown to act as a receptor for SEMA3D and to coimmunoprecipitate with SEMA3D (Foley et al., 2015). In mice, SEMA3C has recently been shown to mediate repulsion of ECs through PLXND1 (Yang et al., 2015). Additionally, Sema3a-PlxnD1 signaling has been shown to guide Se patterning via a repulsive mechanism, leading to ectopic sprouting in either Sema3a- or PlxnD1-deficient embryos (Torres-Vázquez et al., 2004). In contrast to ectopic sprouting induced by Sema3a deficiency, we show here that loss of Sema3d impairs cell migration and cell morphology of Se ECs, which is in line with Nrp1-mediated signaling in the Ses (Fantin et al., 2015).

Many diverse roles of Class III Semaphorins have been published, but difficulties existed in dissecting the various functions mediated by different tissues and receptors in space and time. Sema3d was reported to act as a repellent or an attractant in axon guidance in zebrafish (Wolman et al., 2004; Taku et al., 2016). Accordingly, Moret et al. (2007) studied how intrinsic and extrinsic Sema3a repels and promotes axon migration at the same time. However, our analysis enables us for the first time to dissect these contradictory roles. We show that Sema3d is not only mediating repulsion of ECs but also promoting collective migration of leading edge ECs (Fig. 9 C). Our work reveals a novel mechanism by which EC-specific Sema3d regulates Actin network organization in leading edge ECs. In this case, Sema3d signals through Nrp1 via RhoA and Rock in an autocrine manner, facilitating consistent cell sheet organization. It was shown previously that Sema3d can signal through Nrp1 (Wolman et al., 2004; Moret et al., 2007; Aghajanian et al., 2014). Downstream of Semaphorins, Nrp1 mainly acts as a coreceptor, for instance, acting in combination with Plxn, VegfR, or ErbB2 (Bellon et al., 2010; Gelfand et al., 2014; Fantin et al., 2015; Aghajanian et al., 2016). Further analyses will have to resolve whether Nrp1 interacts with other receptors downstream of Sema3d. Knockdown of NRP1 and 2 in mice severely impairs the developmental yolk sac and embryonic angiogenesis (Takashima et al., 2002). Further, it has been described that NRP1 can control Actin dynamics and that knockdown results in defects in organization of the F-Actin network in HUVECs (Hirota et al., 2015; Yang et al., 2015). However, *plxnD1* knockdown in HUVECs did not affect Actin network organization (Yang et

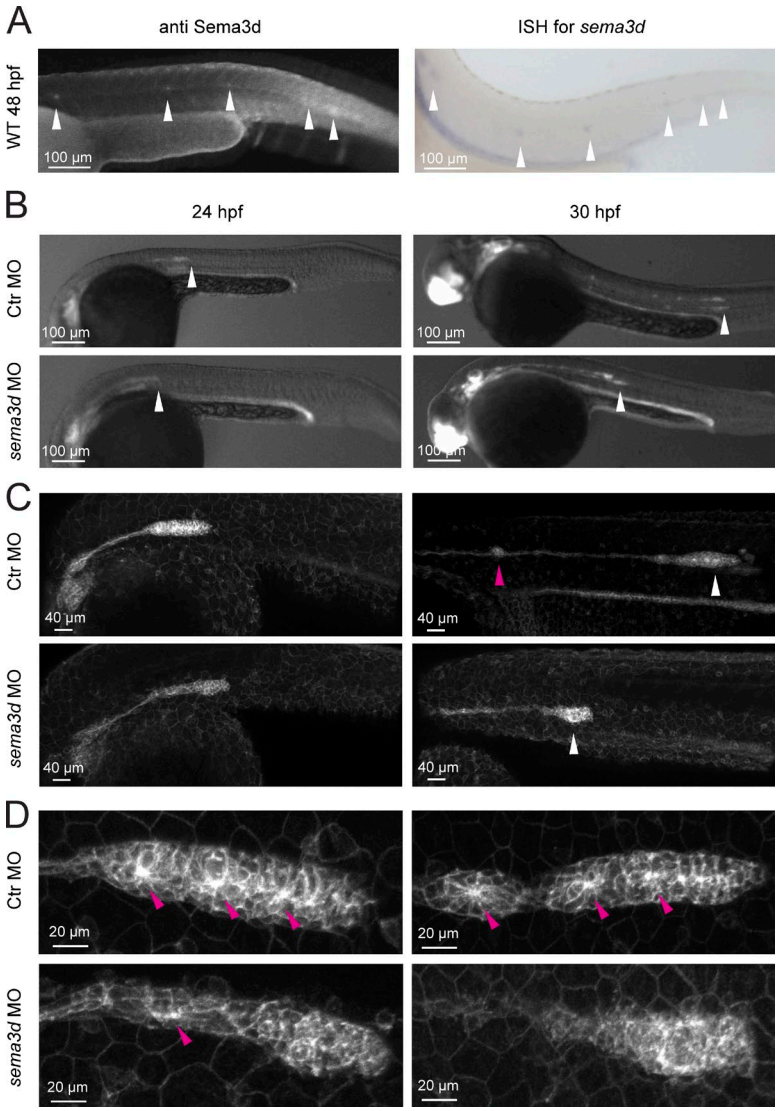

Figure 10. **Collective migration and cell morphology of the LLP are impaired in *sema3d* morphants.** (A) Sema3d antibody staining and in situ hybridization (ISH) for *sema3d* showed Sema3d expression in the LLP and its deposited neuromasts (white arrowheads). (B) LLP migration distance is reduced in *sema3d* morphants at 24 and 30 hpf in *Tg(-8.0cldnb:lynEGFP)*^{zf106} embryos (LLP indicated by white arrowheads). (C) Deposition of neuromasts (pink arrowhead) is impaired in *sema3d* morphants at 30 hpf. (D) Organized LLP rosette structure (pink arrowheads) and cell morphology are impaired in *sema3d* morphants at 24 and 30 hpf.

al., 2015). We show in vivo that Sema3d-Nrp1 signaling controls Actin dynamics in the leading edge cells of collectively migrating CCV ECs, independently of PlxnD1. In accordance with our observations, Sema3d has been shown to affect cytoskeleton reorganization in HUVECs independently of PlxnD1 (Aghajanian et al., 2014). Additionally, we were able to show for the first time that this autocrine EC Sema3d-Nrp1 signaling acts via RhoA and Rock on the Actin network. A previous study (Takamatsu et al., 2010) showed that inhibition of Myosin II or Rock blocked Sema3a-induced dendritic cell migration; however, these components were not placed in a direct signaling pathway. Nevertheless, how Nrp1-Sema3d activity is linked to RhoA-Rock will need further investigations. Recently, Yoshida et al. (2015) showed that Syx, a novel RhoA guanine exchange factor, activates RhoA downstream of Nrp1 signaling. However, because Syx-deficient zebrafish embryos die during gastrulation (Goh and Manser, 2010), we could not test this hypothesis.

We identified Sema3d as a novel regulator of collective migration in different contexts. Collective cell migration is a highly important process during embryogenesis and organogenesis (Scarpa and Mayor, 2016); it also drives processes during tissue repair, immune responses, tissue vascularization, and cancer metastasis (Friedl and Gilmour, 2009). Patients with congenital heart defects and anomalous pulmonary veins have been shown to have disruptions in the Sema3d gene (Silversides et al., 2012; Degenhardt et al., 2013; Sanchez-Castro et al., 2015). Recently, Sema3d autocrine signaling has been shown to promote tumor cell migration (Foley et al., 2015). As we have unraveled the complexity of Sema3d-mediated signaling for regulating collective migration for the first time in vivo, it will be interesting to apply our results to elucidate disease etiology in the future.

Materials and methods

Zebrafish husbandry and strains

Zebrafish (*Danio rerio*) embryos were maintained under standard husbandry conditions at 28.5°C (Westerfield, 2000). Zebrafish strains used were *Tg(kdrl:EGFP)*^{s843} (Jin et al., 2005), *Tg(kdrl:HRAS-mCherry)*^{s896} (Chi et al., 2008), *Tg(-8.0cldnb:lynEGFP)*^{zf106} (Haas and Gilmour, 2006), and *Tg(hsp70:sema3dGFP)* (obtained from M.C. Halloran, University of Wisconsin, Madison, WI; Liu et al., 2004). The following zebrafish mutants were used: *cdh5*^{ubs8} (Lenard et al., 2013), *nrp1a*^{hu10012} (de Bruin et al., 2016), and *kdrl*^{hu5088} (Bussmann et al., 2010).

Generation of *sema3d* mutants by CRISPR/Cas9-mediated mutagenesis

Annealed CRISPR target site primers (CRI*sema3d* SE, 5′-TAGGAG ACAGGTCAGGACGGGA-3′, and AS, 5′-AAACTCCCGTCCTGA CCTGTCT-3′) were cloned into the guide RNA (gRNA) expression vector pDR274 as previously described (Hwang et al., 2013). After DraI digestion (New England Biolabs, Inc.), gRNA was transcribed using MEGAshortscript T7 kit (Ambion). *Nls-zCas9-nls* mRNA was synthesized as previously described (Jao et al., 2013). 2 nl of *sema3d* gRNA (12.5 ng/µl) and *nls-zCas9-nls*-mRNA (300 ng/µl) were injected into one-cell-stage zebrafish embryos. *sema3d* mutant genotypes were analyzed by PCR using *sema3d*geno SE, 5′-CTGCCGAAGCAAATC TCCTA-3′, and AS, 5′-ATATGCCGCACATCCCCTAT-3′, followed by restriction digestion with Hpy188III (New England Biolabs, Inc.).

Generation of *Tg(fli1a:lifeactEGFP)^{mu240}*

The *fli1a:lifeactEGFP* plasmid was generated via gateway cloning using Lifeact-EGFP (Riedl et al., 2008) and pTolfli1epDest (Villefranc et al., 2007). Transgenesis was done as previously described (Helker et al., 2013).

Microinjections

MOs were obtained from Gene Tools. 2 nl containing 3 ng *sema3d* AS-MO, 5′-CATGATGGACGAGGAGATTTCTGCA-3′ (Liu et al., 2004); 3 ng *nrp1a/b* MO, 5′-GAATCCTGGAGTTCGGAGTGC GGAA-3′ (Fantin et al., 2015; previously published as an *nrp1a* MO [Lee et al., 2002]); 7.5 ng *nrp1a* MO, 5′-GAGGATCAACACTAATCC ACAATGC-3′ (Yu and Moens, 2005); 2.5 ng *plxnD1* MO, 5′-CAC ACACACTCACGTTGATGATGAG-3′ (Torres-Vázquez et al., 2004); 3 ng *vegfaa* MO, 5′-CTCGTCTTATTTCCGTGACTGTTTT-3′ (Ober et al., 2004); 3 ng *vegfab* MO, 5′-GGAGCACGCGAACAGCAA AGTTCAT-3′ (Bahary et al., 2007); 3 ng *kdrl* MO, 5′-CCGAATGAT ACTCCGTATGTCAC-3′ (Habeck et al., 2002); and the appropriate amount of standard control MO, 5′-CCTCTTACCTCAGTTACAATT TATA-3′, was injected into the yolk of one-cell-stage embryos. For photo-MO experiments, 4.4 ng *sema3d* SE-photo-MO, 5′-TGCAGA AATCTCPTCGTCCAT-3′, was paired with 4 ng *sema3d* AS-MO (P indicates photo-cleavable linkage).

For overexpression, *sema3d* was PCR-amplified from 24 hpf cDNA and cloned into the pCS2+ vector using primers *sema3d*mRNA SE, 5′-ATGAAGACTGCAGGGGAGCCG-3′, and AS, 5′-CTAGTG GTGGCGTCGGTTTCTG-3′. The mRNA was transcribed with an SP6 mMessage mMachine kit (Ambion). The 2-nl injection volume contained 300 ng/µl *sema3d* mRNA or 300 ng/µl H2Bcherry Ctr mRNA. For Nrp1 rescue experiments, rat *Nrp1*, *Nrp1Δa* (Sema3-signaling deficient, published as Nrp1Δa1+7), and *Nrp1Δb* (published as Nrp1Δb2; Gu et al., 2002) were cloned into pCS2+ via EcoRI and XhoI. The mRNA was transcribed with an SP6 mMessage mMachine kit. The 2-nl injection volume contained 3 ng *nrp1a/b* MO and 300 ng/µl mRNA. For one-in-16 cell injections, 1 nl of *sema3d* AS-MO injection mix containing 1:100 DiI (Molecular Probes) was injected into one cell of a 16-cell-stage embryo.

Photo-MO cleavage

Photo-MO cleavage was performed as described previously (Tallafuss et al., 2012). After embryos were manually dechorionated, photo-MO cleavage was performed using a stereoscope M165FC (Leica Biosystems) with a UV filter and a zoom of 3.0. Embryos were exposed to UV light for 15 min while being rotated four times.

Whole-mount in situ hybridization

Whole-mount in situ hybridization was performed as described (Thisse and Thisse, 2008). Probes were amplified from 24-hpf cDNA with the following T7 promoter site primers: *sema3d* SE, 5′-TGCACAGGT GCCAAATTTAT-3′, and AS, 5′-GTAATACGACTCACTATAGGA TTTTGCACAAGTGGGCATT-3′; *plxnD1* SE, 5′-ACATCGAGAAGA CGGACCAC-3′, and AS, 5′-GTAATACGACTCACTATAGGCATG AAGAACAGCGCAGGTA-3′; and *nrp1a* SE, 5′-ATGGTGGACATC ACCGATTT-3′, and AS, 5′-GTAATACGACTCACTATAGGTGTT TCTTTGAAAAGGGCATT-3′. The *cdh5* probe was synthesized as described previously (Larson et al., 2004).

Immunohistochemistry

Immunohistochemistry was performed as described previously (Blum et al., 2008) using rabbit anti–zebrafish Cdh5 (Blum et al., 2008), mouse anti–human ZO-1 (Invitrogen), rabbit anti–human Sema3d (Sigma-Aldrich), goat anti–mouse Alexa Fluor 546 (Invitrogen), goat anti–rabbit Alexa Fluor 546 (Invitrogen), and goat anti–rabbit Alexa Fluor 647 (Invitrogen).

Transplantations

Donor *Tg(kdrl:EGFP)^{s843}* embryos were injected with *sema3d* MO and 2.5% Alexa Fluor 647 Dextran (Thermo Fisher Scientific). Cells were transplanted into *Tg(kdrl:HRAS-mCherry)^{s896}* hosts as described previously (Helker et al., 2015).

Pharmacological experiments

Inhibitor treatments were performed on dechorionated embryos from 22 hpf to fixation at 30 hpf using 400 µM ROCK inhibitor H-1152 (Enzo Life Sciences), 100 µM (−)-blebbistatin (Sigma-Aldrich), 24 nM latrunculin A (Sigma-Aldrich), 100 µM Cdc42 inhibitor ML141 (Sigma-Aldrich), 1 mM Rac1 inhibitor (Tocris Bioscience), 50 µM FAK inhibitor 14 (Sigma-Aldrich), 12.5 µM nifedipine (Sigma-Aldrich), 3 µg/ml RhoI inhibitor (Cytoskeleton, Inc.), 5 µg/ml Rho activator II (Cytoskeleton, Inc.), and 1 µM VegfR inhibitor SU5416 (Sigma-Aldrich).

Microscopy, in vivo time-lapse analysis, and statistical analysis

Either 4% PFA-fixed or living embryos were mounted in 0.3% agarose (containing 19.2 mg/l tricaine and 30 mg/l phenylthiourea for living embryos) for imaging. Bright-field and epifluorescence images were acquired with a stereomicroscope M165 FC or M205 C (Leica Biosystems) equipped with a C10600 camera (Hamamatsu Photonics) or a MicroPublisher 5.0 RTV camera (QImaging). For live time-lapse imaging, embryos were kept in a 28.5°C heated chamber. Fluorescent confocal images were acquired using an LSM 780 (ZEISS; objective lens: 20× Plan Apo NA 0.80, 40× LD C Apochromat NA 1.10, or 63× Plan-Apo NA 1.40) or an Sp5 inverted confocal microscope (Leica Biosystems; objective lens: 20× HCX PL S-APO NA 0.50). Imaris 7/8 software (Bitplane) was used to assemble confocal stacks and movies. Imaris 7/8 and Fiji 1.45b (ImageJ) software were used for tracking, length, and angle measurements. Determination of cell migration parameters was performed as described previously (Helker et al., 2013). For all quantifications, SDs and p-values with two-tailed *t* test were calculated using Excel 2011 (Microsoft) and Prism 6 (GraphPad). All error bars indicate SD.

Online supplemental material

Fig. S1 shows genetic and phenotypic details for the *sema3d* mutants and morphants. Fig. S2 shows impaired vascular development in Sema3d-deficient embryos. Fig. S3 shows that Sema3d additionally regulates intersegmental vessel development. Fig. S4 shows that EC-specific Sema3d ensures cohesive EC sheet migration. Fig. S5 shows that Nrp1 signaling in the CCV leading edge requires Sema3 binding, but might not depend on VegfA. It also addresses the involvement of VegfR as a Nrp1 coreceptor. Videos 1 and 2 show normal versus

impaired CCV migration in Ctr morphants (Video 1) versus *sema3d* morphants (Video 2) using *Tg(kdrl:EGFP)*^{s843}. Videos 3 and 4 show detailed analysis of Actin cable formation during CCV migration using the novel *Tg(fli1a:lifeactEGFP)*^{mu240}. Ctr morphants exhibit a cohesive EC sheet with prominent Actin cables (Video 3), whereas *sema3d* morphants exhibit a severely disrupted EC sheet (Video 4). Additional data are available in the JCB DataViewer at http://dx.doi.org/10.1083/jcb.201603100.dv.

Acknowledgments

We thank Stefan Schulte-Merker for critical comments and suggestions on the manuscript. We thank Mary C. Halloran for providing *Tg(hsp70:sema3dGFP)*; Heinz-Georg Belting for the Cdh5 antibody; Arndt Siekmann and Jeroen Bussmann for morpholinos, zebrafish lines, and reagents; Erez Raz for *Tg(-8.0cldnb:lynEGFP)*^{zf106}; and Gu Chenghua and Robert Rosa for providing reagents. We are grateful to Reinhild Bussmann for excellent fish husbandry, Katja Müller for technical assistance, and Stefan Volkery for imaging assistance.

This work was supported by the Deutsche Forschungsgemeinschaft (HE 4585/2-1), the North Rhine-Westphalia "return fellowship" awarded to W. Herzog, and a Graduate School Cells-in-Motion Cluster of Excellence fellowship (EXC 1003 – CiM), University of Muenster, to M.J. Hamm.

The authors declare no competing financial interests.

Submitted: 30 March 2016
Accepted: 20 September 2016

References

Aghajanian, H., C. Choi, V.C. Ho, M. Gupta, M.K. Singh, and J.A. Epstein. 2014. Semaphorin 3d and semaphorin 3e direct endothelial motility through distinct molecular signaling pathways. *J. Biol. Chem.* 289:17971–17979. http://dx.doi.org/10.1074/jbc.M113.544833

Aghajanian, H., Y.K. Cho, L.J. Manderfield, M.R. Herling, M. Gupta, V.C. Ho, L. Li, K. Degenhardt, A. Aharonov, E. Tzahor, and J.A. Epstein. 2016. Coronary vasculature patterning requires a novel endothelial ErbB2 holoreceptor. *Nat. Commun.* 7:12038. http://dx.doi.org/10.1038/ncomms12038

Bahary, N., K. Goishi, C. Stuckenholz, G. Weber, J. Leblanc, C.A. Schafer, S.S. Berman, M. Klagsbrun, and L.I. Zon. 2007. Duplicate VegfA genes and orthologues of the KDR receptor tyrosine kinase family mediate vascular development in the zebrafish. *Blood.* 110:3627–3636. http://dx.doi.org/10.1182/blood-2006-04-016378

Bellon, A., J. Luchino, K. Haigh, G. Rougon, J. Haigh, S. Chauvet, and F. Mann. 2010. VEGFR2 (KDR/Flk1) signaling mediates axon growth in response to semaphorin 3E in the developing brain. *Neuron.* 66:205–219. http://dx.doi.org/10.1016/j.neuron.2010.04.006

Blum, Y., H.G. Belting, E. Ellertsdottir, L. Herwig, F. Lüders, and M. Affolter. 2008. Complex cell rearrangements during intersegmental vessel sprouting and vessel fusion in the zebrafish embryo. *Dev. Biol.* 316:312–322. http://dx.doi.org/10.1016/j.ydbio.2008.01.038

Bussmann, J., F.L. Bos, A. Urasaki, K. Kawakami, H.J. Duckers, and S. Schulte-Merker. 2010. Arteries provide essential guidance cues for lymphatic endothelial cells in the zebrafish trunk. *Development.* 137:2653–2657. http://dx.doi.org/10.1242/dev.048207

Chi, N.C., R.M. Shaw, S. De Val, G. Kang, L.Y. Jan, B.L. Black, and D.Y. Stainier. 2008. Foxn4 directly regulates tbx2b expression and atrioventricular canal formation. *Genes Dev.* 22:734–739. http://dx.doi.org/10.1101/gad.1629408

de Bruin, A., P.W. A Cornelissen, B.C. Kirchmaier, M. Mokry, E. Iich, E. Nirmala, K.H. Liang, A.M. D Végh, K.T. Scholman, M.J. Groot Koerkamp, et al. 2016. Genome-wide analysis reveals NRP1 as a direct HIF1α-E2F7 target in the regulation of motorneuron guidance in vivo. *Nucleic Acids Res.* 44:3549–3566. http://dx.doi.org/10.1093/nar/gkv1471

Degenhardt, K., M.K. Singh, H. Aghajanian, D. Massera, Q. Wang, J. Li, L. Li, C. Choi, A.D. Yzaguirre, L.J. Francey, et al. 2013. Semaphorin 3d signaling defects are associated with anomalous pulmonary venous connections. *Nat. Med.* 19:760–765. http://dx.doi.org/10.1038/nm.3185

Eickholt, B.J., S.L. Mackenzie, A. Graham, F.S. Walsh, and P. Doherty. 1999. Evidence for collapsin-1 functioning in the control of neural crest migration in both trunk and hindbrain regions. *Development.* 126:2181–2189.

Ellertsdóttir, E., A. Lenard, Y. Blum, A. Krudewig, L. Herwig, M. Affolter, and H.G. Belting. 2010. Vascular morphogenesis in the zebrafish embryo. *Dev. Biol.* 341:56–65. http://dx.doi.org/10.1016/j.ydbio.2009.10.035

Fantin, A., A. Lampropoulou, G. Gestri, C. Raimondi, V. Senatore, I. Zachary, and C. Ruhrberg. 2015. NRP1 regulates CDC42 activation to promote filopodia formation in endothelial tip cells. *Cell Reports.* 11:1577–1590. http://dx.doi.org/10.1016/j.celrep.2015.05.018

Feiner, L., A.L. Webber, C.B. Brown, M.M. Lu, L. Jia, P. Feinstein, P. Mombaerts, J.A. Epstein, and J.A. Raper. 2001. Targeted disruption of semaphorin 3C leads to persistent truncus arteriosus and aortic arch interruption. *Development.* 128:3061–3070.

Foley, K., A.A. Rucki, Q. Xiao, D. Zhou, A. Leubner, G. Mo, J. Kleponis, A.A. Wu, R. Sharma, Q. Jiang, et al. 2015. Semaphorin 3D autocrine signaling mediates the metastatic role of annexin A2 in pancreatic cancer. *Sci. Signal.* 8:ra77. http://dx.doi.org/10.1126/scisignal.aaa5823

Friedl, P., and D. Gilmour. 2009. Collective cell migration in morphogenesis, regeneration and cancer. *Nat. Rev. Mol. Cell Biol.* 10:445–457. http://dx.doi.org/10.1038/nrm2720

Gammill, L.S., C. Gonzalez, and M. Bronner-Fraser. 2007. Neuropilin 2/semaphorin 3F signaling is essential for cranial neural crest migration and trigeminal ganglion condensation. *Dev. Neurobiol.* 67:47–56. http://dx.doi.org/10.1002/dneu.20326

Gelfand, M.V., N. Hagan, A. Tata, W.J. Oh, B. Lacoste, K.T. Kang, J. Kopycinska, J. Bischoff, J.H. Wang, and C. Gu. 2014. Neuropilin-1 functions as a VEGFR2 co-receptor to guide developmental angiogenesis independent of ligand binding. *eLife.* 3:e03720. http://dx.doi.org/10.7554/eLife.03720

Goh, L.L., and E. Manser. 2010. The RhoA GEF Syx is a target of Rnd3 and regulated via a Raf1-like ubiquitin-related domain. *PLoS One.* 5:e12409. http://dx.doi.org/10.1371/journal.pone.0012409

Gu, C., and E. Giraudo. 2013. The role of semaphorins and their receptors in vascular development and cancer. *Exp. Cell Res.* 319:1306–1316. http://dx.doi.org/10.1016/j.yexcr.2013.02.003

Gu, C., B.J. Limberg, G.B. Whitaker, B. Perman, D.J. Leahy, J.S. Rosenbaum, D.D. Ginty, and A.L. Kolodkin. 2002. Characterization of neuropilin-1 structural features that confer binding to semaphorin 3A and vascular endothelial growth factor 165. *J. Biol. Chem.* 277:18069–18076. http://dx.doi.org/10.1074/jbc.M201681200

Gu, C., Y. Yoshida, J. Livet, D.V. Reimert, F. Mann, J. Merte, C.E. Henderson, T.M. Jessell, A.L. Kolodkin, and D.D. Ginty. 2005. Semaphorin 3E and plexin-D1 control vascular pattern independently of neuropilins. *Science.* 307:265–268. http://dx.doi.org/10.1126/science.1105416

Haas, P., and D. Gilmour. 2006. Chemokine signaling mediates self-organizing tissue migration in the zebrafish lateral line. *Dev. Cell.* 10:673–680. http://dx.doi.org/10.1016/j.devcel.2006.02.019

Habeck, H., J. Odenthal, B. Walderich, H. Maischein, and S. Schulte-Merker. Tübingen 2000 screen consortium. 2002. Analysis of a zebrafish VEGF receptor mutant reveals specific disruption of angiogenesis. *Curr. Biol.* 12:1405–1412. http://dx.doi.org/10.1016/S0960-9822(02)01044-8

Helker, C.S., A. Schuermann, T. Karpanen, D. Zeuschner, H.G. Belting, M. Affolter, S. Schulte-Merker, and W. Herzog. 2013. The zebrafish common cardinal veins develop by a novel mechanism: Lumen ensheathment. *Development.* 140:2776–2786. http://dx.doi.org/10.1242/dev.091876

Helker, C.S., A. Schuermann, C. Pollmann, S.C. Chng, F. Kiefer, B. Reversade, and W. Herzog. 2015. The hormonal peptide Elabela guides angioblasts to the midline during vasculogenesis. *eLife.* 4:e06726. http://dx.doi.org/10.7554/eLife.06726

Hirota, S., T.P. Clements, L.K. Tang, J.E. Morales, H.S. Lee, S.P. Oh, G.M. Rivera, D.S. Wagner, and J.H. McCarty. 2015. Neuropilin 1 balances β8 integrin-activated TGFβ signaling to control sprouting angiogenesis in the brain. *Development.* 142:4363–4373. http://dx.doi.org/10.1242/dev.113746

Hwang, W.Y., Y. Fu, D. Reyon, M.L. Maeder, S.Q. Tsai, J.D. Sander, R.T. Peterson, J.R. Yeh, and J.K. Joung. 2013. Efficient genome editing in zebrafish using a CRISPR-Cas system. *Nat. Biotechnol.* 31:227–229. http://dx.doi.org/10.1038/nbt.2501

Isogai, S., M. Horiguchi, and B.M. Weinstein. 2001. The vascular anatomy of the developing zebrafish: an atlas of embryonic and early larval development. *Dev. Biol.* 230:278–301. http://dx.doi.org/10.1006/dbio.2000.9995

Janssen, B.J., R.A. Robinson, F. Pérez-Brangulí, C.H. Bell, K.J. Mitchell, C. Siebold, and E.Y. Jones. 2010. Structural basis of semaphorin-plexin signalling. *Nature.* 467:1118–1122. http://dx.doi.org/10.1038/nature09468

Jao, L.E., S.R. Wente, and W. Chen. 2013. Efficient multiplex biallelic zebrafish genome editing using a CRISPR nuclease system. *Proc. Natl. Acad. Sci. USA.* 110:13904–13909. http://dx.doi.org/10.1073/pnas.1308335110

Jin, S.W., D. Beis, T. Mitchell, J.N. Chen, and D.Y. Stainier. 2005. Cellular and molecular analyses of vascular tube and lumen formation in zebrafish. *Development.* 132:5199–5209. http://dx.doi.org/10.1242/dev.02087

Kolodkin, A.L., D.J. Matthes, T.P. O'Connor, N.H. Patel, A. Admon, D. Bentley, and C.S. Goodman. 1992. Fasciclin IV: Sequence, expression, and function during growth cone guidance in the grasshopper embryo. *Neuron.* 9:831–845. http://dx.doi.org/10.1016/0896-6273(92)90237-8

Larson, J.D., S.A. Wadman, E. Chen, L. Kerley, K.J. Clark, M. Eide, S. Lippert, A. Nasevicius, S.C. Ekker, P.B. Hackett, and J.J. Essner. 2004. Expression of VE-cadherin in zebrafish embryos: A new tool to evaluate vascular development. *Dev. Dyn.* 231:204–213. http://dx.doi.org/10.1002/dvdy.20102

Lee, P., K. Goishi, A.J. Davidson, R. Mannix, L. Zon, and M. Klagsbrun. 2002. Neuropilin-1 is required for vascular development and is a mediator of VEGF-dependent angiogenesis in zebrafish. *Proc. Natl. Acad. Sci. USA.* 99:10470–10475. http://dx.doi.org/10.1073/pnas.162366299

Lenard, A., E. Ellertsdottir, L. Herwig, A. Krudewig, L. Sauteur, H.G. Belting, and M. Affolter. 2013. In vivo analysis reveals a highly stereotypic morphogenetic pathway of vascular anastomosis. *Dev. Cell.* 25:492–506. http://dx.doi.org/10.1016/j.devcel.2013.05.010

Liu, Y., J. Berndt, F. Su, H. Tawarayama, W. Shoji, J.Y. Kuwada, and M.C. Halloran. 2004. Semaphorin3D guides retinal axons along the dorsoventral axis of the tectum. *J. Neurosci.* 24:310–318. http://dx.doi.org/10.1523/JNEUROSCI.4287-03.2004

Luo, Y., D. Raible, and J.A. Raper. 1993. Collapsin: A protein in brain that induces the collapse and paralysis of neuronal growth cones. *Cell.* 75:217–227. http://dx.doi.org/10.1016/0092-8674(93)80064-L

Meadows, S.M., P.J. Fletcher, C. Moran, K. Xu, G. Neufeld, S. Chauvet, F. Mann, P.A. Krieg, and O. Cleaver. 2012. Integration of repulsive guidance cues generates avascular zones that shape mammalian blood vessels. *Circ. Res.* 110:34–46. http://dx.doi.org/10.1161/CIRCRESAHA.111.249847

Moret, F., C. Renaudot, M. Bozon, and V. Castellani. 2007. Semaphorin and neuropilin co-expression in motoneurons sets axon sensitivity to environmental semaphorin sources during motor axon pathfinding. *Development.* 134:4491–4501. http://dx.doi.org/10.1242/dev.011452

Ober, E.A., B. Olofsson, T. Mäkinen, S.W. Jin, W. Shoji, G.Y. Koh, K. Alitalo, and D.Y. Stainier. 2004. Vegfc is required for vascular development and endoderm morphogenesis in zebrafish. *EMBO Rep.* 5:78–84. http://dx.doi.org/10.1038/sj.embor.7400047

Pellet-Many, C., P. Frankel, H. Jia, and I. Zachary. 2008. Neuropilins: Structure, function and role in disease. *Biochem. J.* 411:211–226. http://dx.doi.org/10.1042/BJ20071639

Püschel, A.W. 2007. GTPases in semaphorin signaling. *Adv. Exp. Med. Biol.* 600:12–23. http://dx.doi.org/10.1007/978-0-387-70956-7_2

Raper, J.A. 2000. Semaphorins and their receptors in vertebrates and invertebrates. *Curr. Opin. Neurobiol.* 10:88–94. http://dx.doi.org/10.1016/S0959-4388(99)00057-4

Riedl, J., A.H. Crevenna, K. Kessenbrock, J.H. Yu, D. Neukirchen, M. Bista, F. Bradke, D. Jenne, T.A. Holak, Z. Werb, et al. 2008. Lifeact: A versatile marker to visualize F-actin. *Nat. Methods.* 5:605–607. http://dx.doi.org/10.1038/nmeth.1220

Sanchez-Castro, M., O. Pichon, A. Briand, D. Poulain, V. Gournay, A. David, and C. Le Caignec. 2015. Disruption of the SEMA3D gene in a patient with congenital heart defects. *Hum. Mutat.* 36:30–33. http://dx.doi.org/10.1002/humu.22702

Sato, M., H.J. Tsai, and H.J. Yost. 2006. Semaphorin3D regulates invasion of cardiac neural crest cells into the primary heart field. *Dev. Biol.* 298:12–21. http://dx.doi.org/10.1016/j.ydbio.2006.05.033

Scarpa, E., and R. Mayor. 2016. Collective cell migration in development. *J. Cell Biol.* 212:143–155. http://dx.doi.org/10.1083/jcb.201508047

Schuermann, A., C.S.M. Helker, and W. Herzog. 2014. Angiogenesis in zebrafish. *Semin. Cell Dev. Biol.* 31:106–114. http://dx.doi.org/10.1016/j.semcdb.2014.04.037

Serini, G., D. Valdembri, S. Zanivan, G. Morterra, C. Burkhardt, F. Caccavari, L. Zammataro, L. Primo, L. Tamagnone, M. Logan, et al. 2003. Class 3 semaphorins control vascular morphogenesis by inhibiting integrin function. *Nature.* 424:391–397. http://dx.doi.org/10.1038/nature01784

Serrels, B., A. Serrels, V.G. Brunton, M. Holt, G.W. McLean, C.H. Gray, G.E. Jones, and M.C. Frame. 2007. Focal adhesion kinase controls actin assembly via a FERM-mediated interaction with the Arp2/3 complex. *Nat. Cell Biol.* 9:1046–1056. http://dx.doi.org/10.1038/ncb1626

Silversides, C.K., A.C. Lionel, G. Costain, D. Merico, O. Migita, B. Liu, T. Yuen, J. Rickaby, B. Thiruvahindrapuram, C.R. Marshall, et al. 2012. Rare copy number variations in adults with tetralogy of Fallot implicate novel risk gene pathways. *PLoS Genet.* 8:e1002843. http://dx.doi.org/10.1371/journal.pgen.1002843

Sit, S.T., and E. Manser. 2011. Rho GTPases and their role in organizing the actin cytoskeleton. *J. Cell Sci.* 124:679–683. http://dx.doi.org/10.1242/jcs.064964

Takamatsu, H., N. Takegahara, Y. Nakagawa, M. Tomura, M. Taniguchi, R.H. Friedel, H. Rayburn, M. Tessier-Lavigne, Y. Yoshida, T. Okuno, et al. 2010. Semaphorins guide the entry of dendritic cells into the lymphatics by activating myosin II. *Nat. Immunol.* 11:594–600. http://dx.doi.org/10.1038/ni.1885

Takashima, S., M. Kitakaze, M. Asakura, H. Asanuma, S. Sanada, F. Tashiro, H. Niwa, J. Miyazaki Ji, S. Hirota, Y. Kitamura, et al. 2002. Targeting of both mouse neuropilin-1 and neuropilin-2 genes severely impairs developmental yolk sac and embryonic angiogenesis. *Proc. Natl. Acad. Sci. USA.* 99:3657–3662. http://dx.doi.org/10.1073/pnas.022017899

Taku, A.A., C.L. Marcaccio, W. Ye, G.J. Krause, and J.A. Raper. 2016. Attractant and repellent cues cooperate in guiding a subset of olfactory sensory axons to a well-defined protoglomerular target. *Development.* 143:123–132. http://dx.doi.org/10.1242/dev.127985

Tallafuss, A., D. Gibson, P. Morcos, Y. Li, S. Seredick, J. Eisen, and P. Washbourne. 2012. Turning gene function ON and OFF using sense and antisense photo-morpholinos in zebrafish. *Development.* 139:1691–1699. http://dx.doi.org/10.1242/dev.072702

Thisse, C., and B. Thisse. 2008. High-resolution in situ hybridization to whole-mount zebrafish embryos. *Nat. Protoc.* 3:59–69. http://dx.doi.org/10.1038/nprot.2007.514

Torres-Vázquez, J., A.D. Gitler, S.D. Fraser, J.D. Berk, V.N. Pham, M.C. Fishman, S. Childs, J.A. Epstein, and B.M. Weinstein. 2004. Semaphorin-plexin signaling guides patterning of the developing vasculature. *Dev. Cell.* 7:117–123. http://dx.doi.org/10.1016/j.devcel.2004.06.008

Villefranc, J.A., J. Amigo, and N.D. Lawson. 2007. Gateway compatible vectors for analysis of gene function in the zebrafish. *Dev. Dyn.* 236:3077–3087. http://dx.doi.org/10.1002/dvdy.21354

Westerfield, M. 2000. The Zebrafish Book. Chapter 3. 4th ed.. University of Oregon Press, Eugene, OR.

Wolman, M.A., Y. Liu, H. Tawarayama, W. Shoji, and M.C. Halloran. 2004. Repulsion and attraction of axons by semaphorin3D are mediated by different neuropilins in vivo. *J. Neurosci.* 24:8428–8435. http://dx.doi.org/10.1523/JNEUROSCI.2349-04.2004

Yang, W.J., J. Hu, A. Uemura, F. Tetzlaff, H.G. Augustin, and A. Fischer. 2015. Semaphorin-3C signals through Neuropilin-1 and PlexinD1 receptors to inhibit pathological angiogenesis. *EMBO Mol. Med.* 7:1267–1284. http://dx.doi.org/10.15252/emmm.201404922

Yoshida, A., A. Shimizu, H. Asano, T. Kadonosono, S.K. Kondoh, E. Geretti, A. Mammoto, M. Klagsbrun, and M.K. Seo. 2015. VEGF-A/NRP1 stimulates GIPC1 and Syx complex formation to promote RhoA activation and proliferation in skin cancer cells. *Biol. Open.* 4:1063–1076. http://dx.doi.org/10.1242/bio.010918

Yu, H.H., and C.B. Moens. 2005. Semaphorin signaling guides cranial neural crest cell migration in zebrafish. *Dev. Biol.* 280:373–385. http://dx.doi.org/10.1016/j.ydbio.2005.01.029